J. Fluid Mech. (2003), *vol.* 487, *pp.* 179–210.
DOI: 10.1017/S0022112003004683 Printed in the United Kingdom

Hydrodynamic theory of premixed flames: effects of stoichiometry, variable transport coefficients and arbitrary reaction orders

By M. MATALON[1], C. CUI[1] AND J. K. BECHTOLD[2]

[1]Department of Engineering Sciences and Applied Mathematics, McCormick School of Engineering and Applied Science, Northwestern University, Evanston, IL 60208-3125, USA

[2]Department of Mathematical Sciences, New Jersey Institute of Technology, Newark, NJ 07102, USA

(Received 26 September 2002)

Based on a hydrodynamic length, which is typically larger than the nominal flame thickness, a premixed flame can be viewed as a surface of density discontinuity, advected and distorted by the flow. The velocities and the pressure suffer abrupt changes across the flame front that consist of Rankine–Hugoniot jump conditions, to leading order, with corrections of the order of the flame thickness that account for transverse fluxes and accumulation. To complete the formulation, expressions for the flame temperature and propagation speed, which vary along the flame as a result of local non-uniformities in the flow field and of flame front curvature, are derived. Unlike previous studies that assumed a mixture consisting of a single deficient reactant, the present study uses a two-reactant scheme and thus considers mixtures whose compositions vary from lean to rich conditions. Furthermore, non-unity and general reaction orders are considered in an attempt to mimic a wider range of reaction mechanisms and, to better represent actual experimental conditions, all transport coefficients are allowed to depend arbitrarily on temperature. The present model, expressed in a coordinate-free form, is valid for flames of arbitrary shape propagating in general fluid flows, either laminar or turbulent.

1. Introduction

One of the complexities in the analysis of combustion problems is the large number of elementary chemical reactions involved in a particular process. It is therefore commonplace in theoretical studies to adopt an overall one-step kinetic model. For premixed flames it is often sufficient to consider a scheme that depends on a single reactant, the deficient one in the mixture. The reaction rate then depends on the concentration of that reactant and, for simplicity, the reaction order is taken to be one. The mixture's properties are characterized by a single Lewis number, defined as the ratio of the thermal diffusivity of the *mixture* (determined primarily by the abundant inert species) to the mass diffusivity of the *deficient* reactant (based on the reactant–inert binary diffusion coefficient). The results apply, therefore, to off-stoichiometric mixtures being either rich or lean and the effective Lewis number is in general significantly different from one:† it is larger than one for lean mixtures

† The Lewis number can be significantly changed by diluting the mixture with an inert that affects primarily the average thermal diffusivity.

of heavy fuels such as hydrocarbons–air (except possibly for methane–air), or rich mixtures of light fuels such as hydrogen–air; it is smaller than one for rich mixtures of heavy fuels or lean mixtures of light fuels. When the fuel and oxidizer in the mixture are nearly at stoichiometric proportions, the mixture properties are better characterized by two Lewis numbers and a scheme that follows both the *fuel* and the *oxidizer* must be considered. Furthermore, to better approximate the effects of the many elementary reactions that actually occur in real systems, the rate of the global reaction must depend on the concentrations of both reactants raised to arbitrary and different powers. The objective of the present study is to use a two-reactant scheme, with arbitrary reaction orders, in order to provide a general hydrodynamic theory of flame propagation in mixtures whose compositions vary from lean to rich.

The propagation of a premixed flame of multidimensional structure in an arbitrary flow field can be described by examining the problem on two separate scales, as carried out by Matalon & Matkowsky (1982) for a single-reactant model. These are the hydrodynamic scale L that characterizes the size of the flame (e.g. the wavelength of wrinkles on the flame front or the geometrical dimensions of the vessel within which the flame propagates), and the diffusion length scale $L_D = \mathscr{D}_{th}/S_L$ that characterizes the thermal thickness of the flame; here $\mathscr{D}_{th}$ is the thermal diffusivity of the mixture and S_L is the laminar flame speed. Typically $L_D \sim 10^{-2}$ cm and L is at least of the order of a few centimetres implying that the ratio $\delta \equiv L_D/L$ is much smaller than one. Viewed on the hydrodynamic length scale, the flame may be regarded as a surface of density discontinuity, advected and distorted by the flow. The flow field (whether laminar or turbulent) is determined by a global analysis where the hydrodynamic equations must be solved subject to jump relations across the flame and appropriate conditions along the boundary of the domain. The flame is characterized by its temperature T_f and propagation speed S_f, which vary along the front as a result of local non-uniformities in flow field and curvature and, in the present study, as a result of deviation from stoichiometry as well. These, and the jump relations in pressure and velocities across the front, remain to be determined from an analysis of the internal structure of the flame.

Unlike the derivation in Matalon & Matkowsky (1982), we use in the present work intrinsic curvilinear coordinates attached to the flame front which not only provide transparent solutions that are more readily interpreted physically, but also cast the results in coordinate-free form that can be easily applied to any geometry of interest. Furthermore, we shall use a two-reactant scheme with arbitrary reaction orders which, in view of the work of Westbrook & Dryer (1981), can represent a wide range of reaction mechanisms; the reaction orders need not necessarily be integers and can often take negative values. Finally, to better represent actual experimental conditions for which the diffusion coefficients tend to increase with temperature through the flame zone, we have allowed all transport coefficients to depend arbitrarily on temperature while retaining the Prandtl and Lewis numbers fixed.

In addition to determining the velocity and pressure fields, we also examine the production of vorticity in the flame zone. Although it is a straightforward matter to deduce the vorticity field and, in particular, the vorticity jump across the flame front once the velocity field is known, we have constructed explicit solutions for the vorticity inside the flame zone that clearly illustrate the roles of viscous diffusion and baroclinic effects and more readily identify the mechanism of vorticity generation. The results have been examined for simple flow configurations.

Among the earlier studies that have used a two-reactant model are the works of Sen & Ludford (1979) and Mitani (1980) who examined the dependence of the

laminar flame speed on stoichiometry, and of Joulin & Mitani (1981) and Jackson (1987) who studied the stability of a planar flame in the context of a constant density model. Effects of variable transport, which are easily accounted for when studying the structure of a planar flame, have been incorporated in more general circumstances by Clavin & Garcia (1983) when examining the stability of a premixed flame and by Keller & Peters (1994) when examining transient pressure effects on the evolution of premixed flames. Both effects were included in the slowly varying-flame analysis of stretched flames by Bechtold & Matalon (1999).

The present theory has numerous applications that complement those previously recognized following the earlier study of Matalon & Matkowsky (1982). First, it provides a general formulation for numerically simulating the propagation of a thin flame, treated as a free boundary, in a general flow field. In particular, it provides explicit expressions for the flame speed and temperature and their dependence on flame stretch, results that have been verified and exploited experimentally by many investigators: cf. Wu & Law (1984), Echekki & Mungal (1990), Kwon, Tseng & Faeth (1992). Second, it is an appropriate framework in which to study the stability characteristics of premixed flames and the onset of cellular or other corrugated structures: cf. Pelce & Clavin (1982), Matalon & Matkowsky (1984), Clavin & Garcia (1983), Bechtold & Matalon (1987), Kim & Matalon (1990). These stability predictions have provided convenient means for comparing theory with experiment as carried out, for example, by Quinard, Searby & Boyer (1984) for planar flames using the results of Pelce & Clavin (1982) and Matalon & Matkowsky (1984), and by Bradley & Harper (1994) and Bradley (1999) for spherical flames using the results of Bechtold & Matalon (1987). Furthermore, the results are applicable to turbulent flames in the flamelet regime, where the entire flame is embedded within eddies of the size of the Kolmogorov scale and the flow within the thin flame is quasi-laminar. This important regime of turbulent combustion, which includes many applications, such as the spark ignition engine, and most laboratory experiments has been rigorously studied by Peters (2000). In all these applications the present study will provide greater quantitative accuracy, by allowing temperature-dependent transport properties, over a wider range of experimental conditions spanning from lean to rich mixtures.

2. Formulation

We consider a premixed flame propagating through a combustible mixture consisting of deficient, $\mathscr{M}_D$, and excess, $\mathscr{M}_E$, reactants, both appearing in relatively small quantities relative to an abundant inert. The reactants mass fractions are Y_{i_u}, for $i = E, D$, where the subscript u denotes conditions in the fresh unburned state. The chemical reaction proceeds according to

$$\nu_D \mathscr{M}_D + \nu_E \mathscr{M}_E \rightarrow \text{Products},$$

where ν_i is the stoichiometric coefficient of species i. The reaction rate obeys an Arrhenius law with an overall activation energy E and a pre-exponential factor $\mathscr{B}$. The reaction orders are taken to be a and b with respect to the deficient/excess reactant, respectively. The ratio of the mass of excess-to-deficient reactants in the fresh mixture is $\Phi = Y_{E_u}/\nu Y_{D_u}$ where $\nu = \nu_E W_E/\nu_D W_D$ is the mass-weighted stoichiometric coefficient ratio, with W_i the molecular weight of species i. We note that Φ is always greater than unity; it is equal to the equivalence ratio for fuel-rich mixtures, and its reciprocal for fuel-lean mixtures.

The density and pressure of the mixture are scaled with respect to their values in the fresh mixture, $\tilde{\rho}_{\rm u}$ and $\tilde{p}_{\rm u}$ (here and in the following symbols with the tilda correspond to a dimensional quantity). The viscosity $\tilde{\mu}$ and thermal conductivity $\tilde{\lambda}$ of the mixture, and the mass diffusivities $\tilde{D}_i$ of the two reactants, depend on the temperature $\tilde{T}$ and are scaled with respect to their values at the temperature $\tilde{T}_{\rm u}$ of the fresh mixture. Although the dependence on temperature is arbitrary, the ratios consisting of the Lewis $Le_i = \tilde{\lambda}/c_p\tilde{\rho}\tilde{D}_i$, and Prandtl $Pr = \tilde{\mu}c_p/\tilde{\lambda}$ numbers, are assumed constant, so that

$$\frac{\tilde{\lambda}}{\tilde{\lambda}_{\rm u}} = \frac{\tilde{\rho}\tilde{D}_i}{\tilde{\rho}_{\rm u}\tilde{D}_{i_{\rm u}}} = \frac{\tilde{\mu}}{\tilde{\mu}_{\rm u}} \equiv \lambda.$$

While this assumption is adopted primarily because of mathematical convenience, we note that for gases $\tilde{\mu}, \tilde{\rho}\tilde{D}_i, \tilde{\lambda} \sim T^{\alpha}$ with $1/2 \leqslant \alpha \leqslant 1$ (Williams 1985) so that the Lewis and Prandtl numbers are nearly constant. Let θ denote the difference of the local temperature from its value in the fresh mixture, scaled with respect to $QY_{D_{\rm u}}/(c_p\nu_D W_D)$ where Q is the heat of combustion and c_p the specific heat (at constant pressure) assumed constant. Then $\theta = (\tilde{T} - \tilde{T}_{\rm u})/(\tilde{T}_a - \tilde{T}_{\rm u})$ where $\tilde{T}_a$ is the adiabatic flame temperature. Lengths and time are scaled on L and L/S_L, respectively, where S_L is the adiabatic flame speed.

The governing equations are the zero-Mach-number Navier–Stokes equations for a variable-density gas mixture, supplemented by the energy equation, mass balance equations for the two reactants and a suitable equation of state. In dimensionless form these are

$$\frac{\partial \rho}{\partial t} + \nabla\cdot(\rho \boldsymbol{v}) = 0, \tag{2.1}$$

$$\rho\frac{\mathrm{D}\boldsymbol{v}}{Dt} = -\nabla p + \delta Pr\,\nabla\cdot\lambda\boldsymbol{\Sigma}, \tag{2.2}$$

$$\rho\frac{\mathrm{D}\theta}{Dt} - \delta\nabla\cdot(\lambda\nabla\theta) = \delta^{-1}\varpi, \tag{2.3}$$

$$\rho\frac{\mathrm{D}Y_D}{Dt} - \delta Le_D^{-1}\nabla\cdot(\lambda\nabla Y_D) = -\delta^{-1}Y_{D_{\rm u}}\varpi, \tag{2.4}$$

$$\rho\frac{\mathrm{D}Y_E}{Dt} - \delta Le_E^{-1}\nabla\cdot(\lambda\nabla Y_E) = -\delta^{-1}\nu Y_{D_{\rm u}}\varpi, \tag{2.5}$$

$$\rho\{1 + (\sigma - 1)\theta\} = 1, \tag{2.6}$$

where $\mathrm{D}/\mathrm{D}t \equiv \partial/\partial t + \boldsymbol{v}\cdot\nabla$ is the convective derivative with t the time variable, $\boldsymbol{v}$ is the velocity vector, and $\boldsymbol{\Sigma} = 2\boldsymbol{E} - \frac{2}{3}(\nabla\cdot\boldsymbol{v})\boldsymbol{I}$ is the viscous stress tensor. Here $\boldsymbol{I}$ is the unit tensor and $\boldsymbol{E} = \frac{1}{2}\{\nabla\boldsymbol{v} + (\nabla\boldsymbol{v})^{\rm T}\}$ is the rate of strain tensor with the superscript T denoting the transpose (the mixture has been assumed to be a Newtonian gas and the bulk viscosity was set to zero). The reaction rate ϖ is given by

$$\varpi = \mathscr{D}\,\rho^{a+b}Y_D^a Y_E^b \exp\left\{\frac{\beta\sigma(\theta - 1)}{1 + (\sigma - 1)\theta}\right\},$$

where $\sigma \equiv \tilde{\rho}_{\rm u}/\tilde{\rho}_{\rm b}$ is the thermal expansion coefficient (the subscript b denotes the state of the burned gas), $\beta = E(\tilde{T}_a - \tilde{T}_{\rm u})/R^o\tilde{T}_a^2$ is the Zeldovich number and $\mathscr{D}$ is the Damköhler number. If the large-activation-energy ($\beta \gg 1$) expression for the laminar

flame speed

$$S_L = \left\{ \frac{2\,(\tilde{\lambda}_\mathrm{b}/c_p)\;\mathscr{G}(a,b;\varphi/Le_E)}{\tilde{\rho}_\mathrm{u}^2\,\beta^{a+b+1}} \frac{\nu_E^b\,Y_{D_\mathrm{u}}^{a+b-1}\,\tilde{\rho}_\mathrm{b}^{a+b}}{\nu_D^{b-1}\,W_D^{a+b-1}} Le_D^a\,Le_E^b\,\mathscr{B} \right\}^{1/2} \exp(-E/2R^o\tilde{T}_a)$$

is used in the scaling, the Damköhler number $\mathscr{D}$ takes the form

$$\mathscr{D} = \frac{\sigma^{a+b}\beta^{a+b+1}}{2\,Le_D^a\,Le_E^b\,\mathscr{G}(a,b;\varphi/Le_E)} \frac{\tilde{\lambda}_\mathrm{u}}{\tilde{\lambda}_\mathrm{b}} \frac{\Phi^b}{Y_{D_\mathrm{u}}^a Y_{E_\mathrm{u}}^b}.$$

The coefficient $\mathscr{G}$, which depends on the reaction orders a and b, the excess reactant Lewis number Le_E, and the parameter $\varphi \equiv \beta(\Phi - 1)$ that measures the departure from stoichiometry, is defined as

$$\mathscr{G}(a,b;z) \equiv \int_0^\infty \varsigma^a(\varsigma + z)^b \mathrm{e}^{-\varsigma}\,\mathrm{d}\varsigma.$$

It is always positive and, at stoichiometry, reduces to $\mathscr{G}(a,b;0) = \Gamma(a+b+1)$ where Γ is the gamma function. When $a = b = 1$, $\mathscr{G}(1,1;z) = 2 + z$ and the expression for S_L reduces to those listed in Bechtold & Matalon (1999) for conditions remote from, near and at stoichiometry. Finally, in the homogeneous fresh mixture far upstream we have $\rho = 1$, $\theta = 0$, $p = 0$ and $Y_i = Y_{i_\mathrm{u}}$; other boundary conditions will be discussed in due course.

3. The reaction sheet

A self-consistent asymptotic analysis for large Zeldovich numbers, $\beta \gg 1$, requires using a near-equidiffusional formulation whereby $Le_i^{-1} = 1 - \beta^{-1} le_i$ (cf. Buckmaster & Ludford 1982), and a near-stoichiometric mixture, for which $Y_{E_\mathrm{u}} - \nu Y_{D_\mathrm{u}} = O(\beta^{-1})$. It is then convenient to introduce the enthalpy functions, h_D and h_E, defined from the relations

$$\theta + Y_D/Y_{D_\mathrm{u}} = 1 + \beta^{-1} h_D,$$
$$\theta + Y_E/\nu Y_{D_\mathrm{u}} = 1 + \beta^{-1} h_E,$$

and consider the variables h_i in lieu of Y_i. The enthalpies satisfy the reaction-free equations

$$\rho \frac{\mathrm{D}h_i}{\mathrm{D}t} - \delta \nabla\cdot(\lambda \nabla h_i) = \delta le_i\,\nabla\cdot(\lambda\nabla\theta). \tag{3.1}$$

In the limit $\beta \to \infty$, the chemical reaction is confined to a sheet, $F(\boldsymbol{x}, t) = 0$, where $\theta \sim 1$ so that the flame temperature may be expressed in the form $\theta_f = 1 + \beta^{-1}\hat{\theta}_f^*$. Let $\boldsymbol{n} = \nabla F/|\nabla F|$ be a unit normal to the reaction sheet pointing towards the burned gas, and $V_f = -F_t/|\nabla F|$ the propagation velocity back along the normal. A standard analysis of the $O(\beta^{-1})$ reactive–diffusive layer then yields the following jump relations across the sheet:

$$[\theta] = [h_i] = 0, \qquad \left[\lambda \frac{\partial h_i}{\partial n}\right] = -le_i \left[\lambda \frac{\partial \theta}{\partial n}\right], \tag{3.2}$$

$$\delta \left[\lambda \frac{\partial \theta}{\partial n}\right] = -\left\{ \frac{\mathscr{G}(a,b;|h_E^* - h_D^*|)}{\mathscr{G}(a,b;\varphi)} \right\}^{1/2} \exp(\hat{\theta}_f^*/2), \tag{3.3}$$

$$[\boldsymbol{v}] = 0, \qquad [p] = \tfrac{4}{3} Pr \left[\lambda \frac{\partial}{\partial n} (\boldsymbol{v} \cdot \boldsymbol{n}) \right], \tag{3.4}$$

$$\left[\frac{\partial}{\partial n} \rho (\boldsymbol{v} \cdot \boldsymbol{n} - V_f) \right] = 0, \qquad \left[\frac{\partial}{\partial n} (\boldsymbol{v} \times \boldsymbol{n}) \right] = 0, \tag{3.5}$$

where $\partial/\partial n \equiv \boldsymbol{n} \cdot \nabla$ is the normal derivative, $[\cdot]$ denotes the jump in the quantity, namely the value on the burned side minus that on the unburned side of the sheet, and the superscript $*$ denotes the value on the burned side of the sheet. These jumps allow for either species to be consumed at the sheet, with the quantity $|h_E^* - h_D^*|$ representing the mass fraction of the unconsumed reactant. When the deficient reactant in the fresh mixture $\mathscr{M}_D$ is the one depleted at the sheet, $Y_D^* = 0$, the flame-temperature perturbation is given by $\hat{\theta}_f^* = h_D^*$, and $h_E^* - h_D^*$ determines the mass fraction of $\mathscr{M}_E$. In particular, we note that when the fresh mixture is sufficiently far from stoichiometry the deficient reactant $\mathscr{M}_D$ is always the one depleted since $\mathscr{M}_E$ is in abundance. Indeed, in the limit when both $h_E^* - h_D^*$ and φ are large and $O(\beta)$, the asymptotic relation $\mathscr{G}(a, b; z) \sim \beta^b \Gamma(a+1)$ for $z \sim \beta$ implies that the factor in the square root of (3.3) tends to a constant that is typically absorbed in the Damköhler number, and the single-reactant results are recovered (cf. Matalon & Matkowsky 1982). For conditions sufficiently close to stoichiometry, however, the local concentration of the reactants in the reaction zone, which depends on their mobility in reaching this zone, determines which of the two reactants is depleted (see Bechtold & Matalon 1999). When the slightly excess reactant in the fresh mixture is the heavier of the two reactants, it can be locally deficient in the reaction zone, and thus depleted by the chemical reaction. In this case, $Y_E^* = 0$, the flame-temperature perturbation is $\hat{\theta}_f^* = h_E^*$ and $h_D^* - h_E^*$ determines the mass fraction of $\mathscr{M}_D$.

In the limit $\beta \to \infty$ the problem, therefore, simplifies to solving (2.1)–(2.6) with $\varpi = 0$ on either side of the reaction sheet, subject to the jump relations (3.2)–(3.5) across the sheet. We note that the results so far are applicable even when distances are scaled on the diffusion length L_D, in which case $\delta = 1$, with no separation between the hydrodynamic and diffusion length scales.

4. Intrinsic coordinates attached to the flame

In analysing the internal structure of the flame, it is convenient to introduce a curvilinear coordinate system (ξ_1, ξ_2, n) attached to the reaction sheet $F(\boldsymbol{x}, t) = 0$. Here ξ_1, ξ_2 are the intrinsic surface coordinates aligned, at every instant in time, with the principal directions of curvature at each point of the surface, and n is the distance to the sheet along the normal (see figure 1). Curvilinear coordinates have been used before, for example for boundary layer flow over a general body (see Rosenhead 1963), but the complete three-dimensional equations for a coordinate system attached to a *moving* surface have not been explicitly written down before. We present the relevant details in Appendix B. A similar coordinate system has been adopted by Cheatham & Matalon (2000) in analysing the structure of diffusion flames and by Ida & Miksis (1998) in examining the dynamics of thin films, but only the relevant equations within the approximations they used were specified. A two-dimensional version of these equations also appeared in the discussion of an evolving detonation front by Yao & Stewart (1996).

Let $\boldsymbol{e}_1$ and $\boldsymbol{e}_2$ denote unit vectors tangential to the parametric curves $\xi_2 = \text{const.}$ and $\xi_1 = \text{const.}$, respectively, then $\boldsymbol{n} = \boldsymbol{e}_1 \times \boldsymbol{e}_2$ is a unit normal and the three vectors $\boldsymbol{e}_1, \boldsymbol{e}_2, \boldsymbol{n}$ form an orthogonal triad of unit vectors. The orientation of the coordinates is

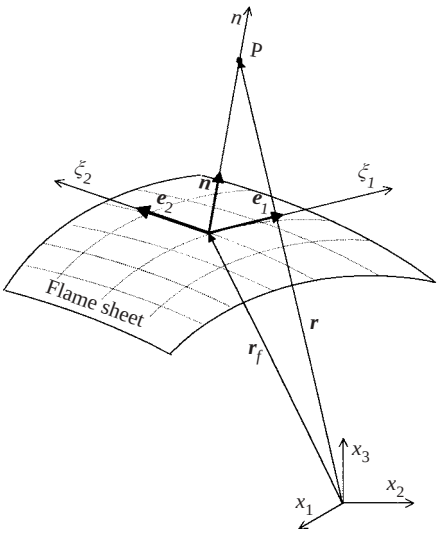

FIGURE 1. The curvilinear coordinates.

chosen such that $\boldsymbol{n}$ points in the direction of the burned gas. The governing equations (2.1)–(2.6) can be expressed in terms of the new coordinate system if the scale factors

$$l_1 = a_1(1 - n\kappa_1), \qquad l_2 = a_2(1 - n\kappa_2), \qquad l_3 = 1$$

are used in the computation of the vector differential operators (see Appendix B), and the transformation

$$\frac{\partial}{\partial t} \mapsto \frac{\partial}{\partial t} + \boldsymbol{q} \cdot \nabla_s - V_f \frac{\partial}{\partial n} \tag{4.1}$$

is used to express time derivatives in the moving frame. (To avoid unnecessary additional notation, the time variable in the moving frame is also denoted by t.) Here κ_1 and κ_2 are the principal curvatures in the ξ_1- and ξ_2-directions, respectively, with $\kappa = \kappa_1 + \kappa_2$ twice the mean curvature of the surface. $V_f = -\partial n/\partial t$ represents the velocity of the surface back along its normal and $\boldsymbol{q} = q_1\boldsymbol{e}_1 + q_2\boldsymbol{e}_2$ with $q_i = l_i\, \partial\xi_i/\partial t$ the time rate of change of an arclength along the coordinate curve ξ_i. We note, in particular, that the gradient operator takes the form

$$\nabla = \boldsymbol{n}\frac{\partial}{\partial n} + \nabla_s, \qquad \nabla_s = \boldsymbol{e}_1 \frac{1}{l_1}\frac{\partial}{\partial \xi_1} + \boldsymbol{e}_2 \frac{1}{l_2}\frac{\partial}{\partial \xi_2},$$

where ∇_s is the surface gradient; all other relevant operators are written down in Appendix B.

We will avoid writing the general equations in the moving curvilinear system and write only the relevant terms at each stage of the analysis. Furthermore, it is convenient in the following development to express the velocity field in directions normal and tangential to the sheet, writing $\boldsymbol{v} = \boldsymbol{v}_\perp + u\,\boldsymbol{n}$, with u the velocity normal to the sheet and $\boldsymbol{v}_\perp = v_1\boldsymbol{e}_1 + v_2\boldsymbol{e}_2$ along the sheet, and introduce $m \equiv \rho(u - V_f)$ as the mass flux normal to the sheet.

5. The flame zone

We consider the limit $\delta \ll 1$ and, consistent with that, assume that $1/\beta \ll \delta$. The flame structure now consists of a reactive–diffusive internal layer with thickness

$\sim O(\delta/\beta)$ embedded inside another internal layer of thickness $\sim O(\delta)$. In the limit $\delta \to 0$ the reaction zone, and the thicker convective–diffusive preheat zone ahead of it, shrink to the surface $F = 0$ that separates the burned products ($F > 0$) from the fresh unburned gas ($F < 0$). The state of the fresh mixture is given by

$$\theta = 0, \quad Y_D = Y_{D_u}, \quad Y_E = Y_{E_u} \qquad \text{for} \quad F < 0, \tag{5.1}$$

corresponding to $h_D = 0$ and $h_E = \varphi$. In the burned gas, the flame temperature perturbation and the concentration of the unconsumed reactant are small as will be verified later. Thus

$$\theta = 1 + O(\delta\beta^{-1}), \quad Y_D = 0, \quad Y_E = Y_{E_u}(\Phi - 1) + O(\delta\beta^{-1}) \qquad \text{for} \quad F > 0. \tag{5.2}$$

We have assumed here that $\mathscr{M}_D$ is the reactant depleted at the reaction sheet, which is always the case when $\varphi = O(1)$; the appropriate modifications needed when $\mathscr{M}_E$ is the depleted reactant will be discussed below.

In the hydrodynamic zones, on either side of the flame, the state of the gas (5.1)–(5.2) is therefore nearly uniform up to and including $O(\delta)$. The flow field is described by incompressible equations: Euler's equations to leading order with viscous effects incorporated as $O(\delta)$ perturbations, but with piecewise-constant density and viscosity: $\rho = 1$, $\lambda = 1$ on the unburned side, and $\rho = 1/\sigma$, $\lambda = \lambda_b$ (corresponding to $\theta = 1$) on the burned side. The velocity field is denoted by $\boldsymbol{v} = \boldsymbol{V}_\perp + U\,\boldsymbol{n}$ where U is the velocity in a direction normal to the flame surface and $\boldsymbol{V}_\perp = V_1\boldsymbol{e}_1 + V_2\boldsymbol{e}_2$ is tangential to the flame surface. The term flame speed is commonly used to refer to the flame velocity relative to the unburned gas and is meaningful only in the asymptotic sense considered here when the location $F = 0$ identifies the flame position unambiguously; thus $S_f = U|_{n=0^-} - V_f$.

To examine the internal structure of the flame zone, we introduce the stretching transformation

$$\eta = \int_0^{n/\delta} \frac{1}{\lambda}\,\mathrm{d}n', \tag{5.3}$$

which implies† that

$$\lambda\frac{\partial}{\partial n} = \frac{1}{\delta}\frac{\partial}{\partial \eta}, \qquad \nabla_s \mapsto \nabla_s + \left(\frac{\partial\lambda}{\partial\theta}\frac{\partial\eta}{\partial\lambda}\nabla_s\theta\right)\frac{\partial}{\partial\eta},$$

and seek solutions in power series of δ, namely of the form $u = u^{(0)} + \delta u^{(1)} + \cdots$. These solutions must then be matched with the solutions in the hydrodynamic regions, accomplished by comparing their behaviour as $\eta \to \pm\infty$ with the corresponding expansion of the outer variables at $n = 0^\pm$. The latter are of the form

$$U \sim U^{(0)}\Big|_{n=0^\pm} + \delta\left\{\frac{\partial U^{(0)}}{\partial n}\bigg|_{n=0^\pm}\int_0^\eta \lambda\,\mathrm{d}\eta' + U^{(1)}\Big|_{n=0^\pm}\right\}$$

and are obtained using a Taylor series expansion near $n = 0$, and the transformation (5.3).

† Note that since, to leading order, the temperature θ is found to depend only on η, $\nabla s \longmapsto \nabla s + O(\delta)$. The $O(\delta)$ term will not be needed in the subsequent analysis.

To leading order the governing equations reduce to

$$\frac{\partial m^{(0)}}{\partial \eta} = 0, \tag{5.4}$$

$$m^{(0)} \frac{\partial \theta^{(0)}}{\partial \eta} - \frac{\partial^2 \theta^{(0)}}{\partial \eta^2} = 0, \tag{5.5}$$

$$m^{(0)} \frac{\partial h_i^{(0)}}{\partial \eta} - \frac{\partial^2 h_i^{(0)}}{\partial \eta^2} = le_i \frac{\partial^2 \theta^{(0)}}{\partial \eta^2}, \tag{5.6}$$

$$m^{(0)} \frac{\partial u^{(0)}}{\partial \eta} = -\frac{\partial p^{(0)}}{\partial \eta} + \frac{4}{3} Pr \frac{\partial^2 u^{(0)}}{\partial \eta^2}, \tag{5.7}$$

$$m^{(0)} \frac{\partial \boldsymbol{v}_\perp^{(0)}}{\partial \eta} = Pr \frac{\partial^2 \boldsymbol{v}_\perp^{(0)}}{\partial \eta^2}. \tag{5.8}$$

Solutions that satisfy the jump conditions (3.2)–(3.5) at $\eta = 0$ and match (5.1)–(5.2) as $\eta \to \pm\infty$, are

$$m^{(0)} = 1, \qquad \boldsymbol{v}_\perp^{(0)} = \left(\boldsymbol{v}_\perp^{(0)}\right)_{-\infty},$$

$$\theta^{(0)} = \begin{cases} \mathrm{e}^\eta \\ 1, \end{cases} \quad \rho^{(0)} = \begin{cases} \{1 + (\sigma - 1)\,\mathrm{e}^\eta\}^{-1}, & \eta < 0 \\ \sigma^{-1}, & \eta > 0, \end{cases}$$

$$h_D^{(0)} = \begin{cases} -le_D\, \eta\, \mathrm{e}^\eta \\ 0 \end{cases}, \quad h_E^{(0)} = \begin{cases} \varphi - le_E\, \eta\, \mathrm{e}^\eta, & \eta < 0 \\ \varphi, & \eta > 0, \end{cases}$$

$$u^{(0)} = \begin{cases} u_{-\infty}^{(0)} + (\sigma - 1)\,\mathrm{e}^\eta, & \eta < 0 \\ u_{-\infty}^{(0)} + \sigma - 1, & \eta > 0, \end{cases}$$

$$p^{(0)} = \begin{cases} p_{-\infty}^{(0)} + \left(\frac{4}{3} Pr - 1\right)(\sigma - 1)\,\mathrm{e}^\eta, & \eta < 0 \\ p_{-\infty}^{(0)} - (\sigma - 1), & \eta > 0, \end{cases}$$

where the subscript $-\infty$ denotes values as $\eta \to -\infty$. Matching the expressions for the pressure and velocities with the solutions in the hydrodynamic regions yields the jump conditions

$$\left[\!\left[U^{(0)}\right]\!\right] = \sigma - 1, \quad \left[\!\left[\boldsymbol{V}_\perp^{(0)}\right]\!\right] = 0, \quad \left[\!\left[P^{(0)}\right]\!\right] = -(\sigma - 1) \tag{5.9}$$

across the flame, where $[\![\cdot]\!] = (\cdot)_{n=0^+} - (\cdot)_{n=0^-}$ denotes the jump. We also obtain that

$$S_f \sim U^{(0)}\Big|_{n=0^-} - V_f^{(0)} = 1, \tag{5.10}$$

which states that, to leading order, the flame speed equals the laminar flame speed. These results will be further discussed below.

The continuity and transport equations for the mass flux, temperature and enthalpies, at the next order, take the form

$$\frac{1}{\lambda} \frac{\partial m^{(1)}}{\partial \eta} = \kappa - \rho^{(0)} K, \tag{5.11}$$

$$\frac{\partial \theta^{(1)}}{\partial \eta} - \frac{\partial^2 \theta^{(1)}}{\partial \eta^2} = -\left(m^{(1)} + \lambda\kappa\right)\frac{\partial \theta^{(0)}}{\partial \eta}, \tag{5.12}$$

$$\frac{\partial h_i^{(1)}}{\partial \eta} - \frac{\partial^2 h_i^{(1)}}{\partial \eta^2} = -\left(m^{(1)} + \lambda\kappa\right)\frac{\partial h_i^{(0)}}{\partial \eta} + le_i\frac{\partial^2 \theta^{(1)}}{\partial \eta^2} - le_i\,\lambda\kappa\frac{\partial \theta^{(0)}}{\partial \eta}, \tag{5.13}$$

where K is the flame stretch given by $K = -V_f\,\kappa + \nabla_s \cdot \boldsymbol{v}_\perp$ (see Appendix A). It can also be expressed, in general, as $K = S_f\,\kappa + K_s$ identifying the separate contributions due to curvature $\kappa = -\nabla\cdot\boldsymbol{n}$ and strain $K_s = -\boldsymbol{n}\cdot\boldsymbol{E}\cdot\boldsymbol{n}$, but in the present context it appears only in the perturbation terms and, since to leading order $S_f \sim 1$, it suffices to use the approximation $K \sim \kappa + K_s$.

Equation (5.11) can be integrated to give

$$m^{(1)} = f_1 + \begin{cases} \kappa I(\eta) - K\,J(\eta), & \eta < 0 \\ (\kappa - \sigma^{-1}K)\,\lambda_{\mathrm{b}}\,\eta, & \eta > 0, \end{cases} \tag{5.14}$$

where $f_1 = f_1(\xi_1, \xi_2, t)$ remains to be determined. Here

$$I(\eta) = -\int_{\Theta}^{\sigma} \frac{\lambda(x)}{x-1}\,\mathrm{d}x, \qquad J(\eta) = -\int_{\Theta}^{\sigma} \frac{\lambda(x)}{x(x-1)}\,\mathrm{d}x,$$

with $\Theta(\eta) = 1 + (\sigma - 1)\mathrm{e}^{\eta}$ and λ_{b} the value of λ at the reaction sheet ($\eta = 0$) or, equivalently, at the state of the burned gas. For simplicity of presentation we will avoid writing the explicit solutions for $\theta^{(1)}$ and $h_i^{(1)}$ and instead quote only the essential results. Integrating (5.12) and (5.13) from $\eta = -\infty$ to $\eta = 0^-$, using the jump conditions (3.2) and the matching conditions as $\eta \to -\infty$, we obtain

$$\left.\frac{\partial \theta^{(1)}}{\partial \eta}\right|_{\eta=0^-} = f_1 + \frac{\gamma_1}{\sigma}K\,, \qquad \left.h_i^{(1)}\right|_{\eta=0} = -le_i\;\gamma_2 K,$$

where

$$\gamma_1 = \frac{\sigma}{\sigma-1}\int_1^{\sigma} \frac{\lambda(x)}{x}\,\mathrm{d}x, \qquad \gamma_2 = \frac{1}{\sigma-1}\int_1^{\sigma} \frac{\lambda(x)}{x}\ln\left(\frac{\sigma-1}{x-1}\right)\mathrm{d}x.$$

Finally, by applying the jump relation (3.3) we find that $f_1 = (-\alpha + \gamma_1(\sigma-1)/\sigma)\,K$ with $\alpha = \gamma_1 + \frac{1}{2}le_{\mathrm{eff}}\,\gamma_2$ expressed in terms of an 'effective' reduced Lewis number

$$le_{\mathrm{eff}} = le_D + (le_E - le_D)\frac{b\,\mathscr{G}(a, b-1; \varphi)}{\mathscr{G}(a, b; \varphi)}.$$

We note that the local concentration difference at the reaction sheet, which is proportional to $h_E^* - h_D^* = \varphi - \delta(le_E - le_D)\,\gamma_2 K$, is always positive when $\varphi = O(1)$ implying that the deficient reactant in the fresh mixture is the one depleted. When $\varphi = O(\delta)$ it is the sign of the right-hand side of this equality that determines which of the two reactants is totally consumed; when positive $\mathscr{M}_D$ is totally consumed and consequently $\hat{\theta}_f^* = h_D^*$, when negative $\mathscr{M}_E$ is totally consumed and consequently $\hat{\theta}_f^* = h_E^*$. This ensures that the concentration of the unconsumed reactant $|h_E^* - h_D^*|$ is always positive, as it should be. When applied to the jump condition (3.3), the same results for f_1 and α are obtained in either case, so that the flow field and flame speed are unaffected by these small modifications.

The $O(\delta)$ correction to the normal velocity ahead of the flame can now be deduced from (5.14) and the equation of state (2.6), by taking the limit $\eta \to -\infty$; we find

$$U^{(1)}\Big|_{n=0^-} - V_f^{(1)} = -\alpha K \tag{5.15}$$

along with the jump relations

$$[\![U^{(1)}]\!] = -\tfrac{1}{2}(\sigma-1)\gamma_2 l e_{\text{eff}} K, \qquad \left[\!\!\left[\frac{\partial U^{(0)}}{\partial n}\right]\!\!\right] = (\sigma-1)\kappa. \tag{5.16}$$

The momentum equations to $O(\delta)$ take the form

$$Pr\frac{\partial^2 \boldsymbol{v}_\perp^{(1)}}{\partial \eta^2} - \frac{\partial \boldsymbol{v}_\perp^{(1)}}{\partial \eta} = \lambda\left\{\tilde{\nabla}_s p^{(0)} + \rho^{(0)} \mathrm{D}_\perp^* \boldsymbol{v}^{(0)} - Pr\frac{1}{\lambda}\frac{\partial \lambda}{\partial \eta}\left(\boldsymbol{w}^{(0)} + \tilde{\nabla}_s u^{(0)}\right)\right\}, \tag{5.17}$$

$$\begin{aligned}\frac{\partial p^{(1)}}{\partial \eta} = &-\frac{\partial u^{(1)}}{\partial \eta} - m^{(1)}\frac{\partial u^{(0)}}{\partial \eta} - \lambda \rho^{(0)} \mathrm{D}_n^* \boldsymbol{v}^{(0)} + \lambda \frac{\partial u^{(0)}}{\partial \eta} \\ &+ \frac{4}{3}Pr\left(\frac{\partial^2 u^{(1)}}{\partial \eta^2} - \lambda\kappa\frac{\partial u^{(0)}}{\partial \eta}\right) + \frac{2}{3}Pr\frac{\partial \lambda}{\partial \eta}\left\{\left(u^{(0)} - V_f^{(0)}\right)\kappa - K\right\},\end{aligned} \tag{5.18}$$

where $\mathrm{D}_\perp^* \boldsymbol{A} \equiv (\mathrm{D}\boldsymbol{A}/\mathrm{D}t)_\perp$ and $\mathrm{D}_n^* \boldsymbol{A} \equiv (\mathrm{D}\boldsymbol{A}/\mathrm{D}t)_n$ stand for the transverse and normal components of the material derivative of the vector $\boldsymbol{A}$ as defined in (B 16), $\tilde{\nabla}_s$ stands for the leading term of the surface gradient, obtained simply by replacing l_i in ∇_s with a_i, $\boldsymbol{w}^{(0)} \equiv \kappa_1 v_1^{(0)} \boldsymbol{e}_1 + \kappa_2 v_2^{(0)} \boldsymbol{e}_2$, and $\boldsymbol{v}^{(0)} = \boldsymbol{v}_\perp^{(0)} + u^{(0)}\boldsymbol{n}$.

Although these equations can be easily integrated to construct explicit solutions for $\boldsymbol{v}_\perp^{(1)}$ and $p^{(1)}$, the algebra is quite tedious and the details are of little interest. In order to obtain the jump conditions for the corresponding outer variables across the flame it suffices to integrate these equations once; matching with the solutions in the hydrodynamic regions then yields

$$[\![\boldsymbol{V}_\perp^{(1)}]\!] = \left(\gamma_1 + \frac{\sigma - \lambda_\mathrm{b}}{\sigma - 1}Pr\right)\left[\!\!\left[\frac{\partial \boldsymbol{V}_\perp^{(0)}}{\partial n}\right]\!\!\right] + (\lambda_\mathrm{b} - 1)\,Pr\left\{\tilde{\nabla}_s\left(2U^{(0)} - P^{(0)}\right) + 2\boldsymbol{W}^{(0)}\right\}, \tag{5.19}$$

$$[\![P^{(1)}]\!] = \gamma_1\left[\!\!\left[\frac{\partial P^{(0)}}{\partial n}\right]\!\!\right] + (\sigma-1)\gamma_2 l e_{\text{eff}}\, K - 2(\lambda_\mathrm{b} - 1)Pr\, K_s + \Gamma\kappa, \tag{5.20}$$

where $\boldsymbol{W} \equiv \kappa_1 V_1 \boldsymbol{e}_1 + \kappa_2 V_2 \boldsymbol{e}_2$ and

$$\Gamma = (\sigma-1)\gamma_1 - (2Pr - 1)\gamma_3 + 2Pr(\sigma-1)\lambda_\mathrm{b}, \qquad \gamma_3 = \int_1^\sigma \lambda(x)\,\mathrm{d}x.$$

As a matter of convention, here and hereafter, all terms on the right-hand side in jump relations across $n = 0$ are to be evaluated at $n = 0^-$. We also find that

$$\left[\!\!\left[\frac{\partial \boldsymbol{V}_\perp^{(0)}}{\partial n}\right]\!\!\right] = \frac{\sigma - 1}{\sigma}\left\{\mathrm{D}_\perp^* \boldsymbol{V}^{(0)} - \frac{\partial \boldsymbol{V}_\perp^{(0)}}{\partial n} + \left(\boldsymbol{W}^{(0)} + \tilde{\nabla}_s U^{(0)}\right)\right\},$$

$$\left[\!\!\left[\frac{\partial P^{(0)}}{\partial n}\right]\!\!\right] = -(\sigma-1)\kappa + \frac{\sigma-1}{\sigma}\left(\mathrm{D}_n^* \boldsymbol{V} - \frac{\partial U^{(0)}}{\partial n}\right),$$

where $\boldsymbol{V}^{(0)} = \boldsymbol{V}_\perp^{(0)} + U^{(0)}\boldsymbol{n}$, but these, like (5.16), do not provide new information;

they can be obtained equivalently by integrating the Euler equations, valid in the hydrodynamic regions, across the flame surface.

6. The hydrodynamic model

The derivation in the previous section shows that, when $\delta \ll 1$, a premixed flame can be treated as a surface of density discontinuity. The problem then simplifies to a hydrodynamic free-boundary problem. On either side of the flame sheet, described by $F(\boldsymbol{x}, t) = 0$, the Euler equations with viscous correction terms must be satisfied, but with different densities and viscosities. Hence

$$\nabla \cdot \boldsymbol{v} = 0, \tag{6.1}$$

$$\rho \frac{\mathrm{D}\boldsymbol{v}}{\mathrm{D}t} = -\nabla p + \delta Pr\, \nabla \cdot \lambda(\nabla \boldsymbol{v} + \nabla \boldsymbol{v}^{\top}), \tag{6.2}$$

with

$$\rho = \begin{cases} 1 \\ 1/\sigma, \end{cases} \quad \lambda = \begin{cases} 1, & F < 0 \\ \lambda_{\mathrm{b}}, & F > 0. \end{cases} \tag{6.3}$$

The jump conditions that must be satisfied across the flame are obtained by combining the results (5.9) and (5.16)–(5.20). Correct to $O(\delta)$ these conditions can be written as

$$[\![\rho(\boldsymbol{v}\cdot\boldsymbol{n} - V_f)]\!] = \delta \frac{\sigma - 1}{\sigma}\, \gamma_1 K, \tag{6.4}$$

$$[\![\boldsymbol{n} \times (\boldsymbol{v} \times \boldsymbol{n})]\!] = \delta \left\{ -(\lambda_{\mathrm{b}} Pr + \gamma_1)[\![\boldsymbol{n} \times (\nabla \times \boldsymbol{v})]\!] + 2Pr\,(\lambda_{\mathrm{b}} - 1)\, (\boldsymbol{n} \times (\boldsymbol{E}\cdot\boldsymbol{n}) \times \boldsymbol{n}) \right\}, \tag{6.5}$$

$$\begin{aligned} &[\![p + \rho(\boldsymbol{v}\cdot\boldsymbol{n})(\boldsymbol{v}\cdot\boldsymbol{n} - V_f)]\!] \\ &\quad = \delta \left\{ \gamma_1\, [\![\boldsymbol{n}\cdot\nabla p]\!] + \frac{\sigma - 1}{\sigma} \gamma_1 V_f\, K + \Gamma\, \kappa + 2Pr(\lambda_{\mathrm{b}} - 1)\, (\boldsymbol{n}\cdot\boldsymbol{E}\cdot\boldsymbol{n}) \right\}, \end{aligned} \tag{6.6}$$

with the right-hand side evaluated at $n = 0^{-}$. The equation for the flame speed $S_f \equiv \boldsymbol{v}\cdot\boldsymbol{n} - \boldsymbol{V}_f$ that completes the formulation is obtained by combining (5.10) and (5.15), to give

$$S_f = 1 - \delta\alpha\, K, \tag{6.7}$$

with

$$\alpha = \frac{\sigma}{\sigma - 1} \int_1^{\sigma} \frac{\lambda(x)}{x}\, \mathrm{d}x + \frac{\beta(Le_{\mathrm{eff}} - 1)}{2(\sigma - 1)} \int_1^{\sigma} \frac{\lambda(x)}{x} \ln\left(\frac{\sigma - 1}{x - 1}\right) \mathrm{d}x. \tag{6.8}$$

Equation (6.7) can alternatively be thought of as an equation for the flame surface F. Here $\boldsymbol{n}$ is the unit normal to the flame surface pointing in the direction of the burned gases, V_f is the normal velocity of the surface and $\kappa = -\nabla\cdot\boldsymbol{n}$ its curvature, and K is the flame stretch. See Appendix A for general expressions for K in coordinate-free form.

We note that spatial and temporal density variations in the burned gas region, resulting from the temperature perturbations, are $O(\delta\beta^{-1})$ and thus much smaller in magnitude. Similarly, variations in the concentration of the unconsumed reactant in the burned gas are also $O(\delta\beta^{-1})$. These can, therefore, be determined *a posteriori* by

solving

$$\rho \frac{\mathrm{D}Y}{\mathrm{D}t} = 0, \qquad \rho \frac{\mathrm{D}\theta}{\mathrm{D}t} = 0, \tag{6.9}$$

subject to

$$Y^* = \beta^{-1} Y_{\mathrm{u}} \left| \varphi + \delta(le_D - le_E)\, \gamma_2\, K \right|, \tag{6.10}$$

$$\theta_f = \begin{cases} 1 - \delta\beta^{-1} le_D\, \gamma_2\, K & \text{when } Y_D^* = 0 \\ 1 - \beta^{-1}(\delta le_E\, \gamma_2\, K - \varphi) & \text{when } Y_E^* = 0 \end{cases} \tag{6.11}$$

at $n = 0^+$. Here Y^* denotes the mass fraction of the unconsumed reactant that leaks through the reaction zone, determined by the sign of the quantity within the absolute value in (6.10), and θ_f is the flame temperature. When $\varphi = O(1)$, the deficient reactant in the fresh mixture is also the one that is locally deficient in the reaction zone; then $Y_D^* = 0$ and $Y^* = Y_E^*$. The same is true when $\varphi = O(\delta)$ provided $\varphi + \delta(le_D - le_E)\, \gamma_2\, K > 0$. Otherwise the excess reactant in the fresh mixture is locally deficient in the reaction zone, $Y_E^* = 0$ and $Y^* = Y_D^*$. The flame temperature always depends on the enthalpy of the reactant that is being totally consumed.

The model presented here is a generalization of the results of Matalon & Matkowsky (1982, 1983), for mixtures spanning the whole range from lean to rich conditions, with arbitrary reaction orders and temperature-dependent transport properties. Their results† can be easily recovered by setting $\lambda_{\mathrm{b}} = 1$, so that

$$\gamma_1 = \frac{\sigma}{\sigma - 1} \ln \sigma, \quad \gamma_2 = \frac{1}{\sigma - 1} \int_{-\infty}^{0} \ln \left\{ 1 + (\sigma - 1) \mathrm{e}^{z} \right\} \mathrm{d}z, \quad \gamma_3 = \sigma - 1,$$

and by interpreting le_{eff} as being associated with the deficient component in the mixture. We note the presence of an 'effective' Prandtl number, λPr, which increases through the flame as a result of the increase in temperature, appearing in the momentum equations and producing changes in the rate of strain that contribute to the overall momentum jump across the flame. Variations in thermal and mass diffusivities with temperature appear in the coefficients γ_1, γ_2 and α. The importance of incorporating these effects in studies of flame dynamics will be illustrated below for simple flame configurations.

The jump conditions (6.4)–(6.6) across the flame, representing changes in mass and momentum, consist of Rankine–Hugoniot conditions to leading order, with corrections of the order of the flame thickness that account for transverse fluxes and accumulation. Here too, the terms corresponding to the strain rate are modified by the change in viscosity through the flame.

The flame speed relation (6.7) reiterates its linear dependence on stretch (Matalon & Matkowsky 1982), with a coefficient α known as the Markstein number. With the effective Lewis number Le_{eff} for the mixture, given by

$$Le_{\mathrm{eff}} = \frac{Le_E + Le_D \mathscr{A}}{1 + \mathscr{A}}, \qquad \mathscr{A} \equiv \frac{\mathscr{G}(a, b; \varphi)}{b\, \mathscr{G}(a, b - 1; \varphi)} - 1, \tag{6.12}$$

† There were some typographical and minor errors in these publications: In Matalon & Matkowsky (1982) the second term in the curly bracket on the right-hand side of (6.12), and equivalently in (A 2) of the appendix in Matalon & Matkowsky (1983), should have a + sign. Further, in Matalon & Matkowsky (1983), there is a wrong sign in (A 5) and as a result (A 11) should include the additional term $q\nabla \times \boldsymbol{n}$ on its right-hand side. Consequently the second term in the curly bracket on the right-hand side of (3.13) should be removed.

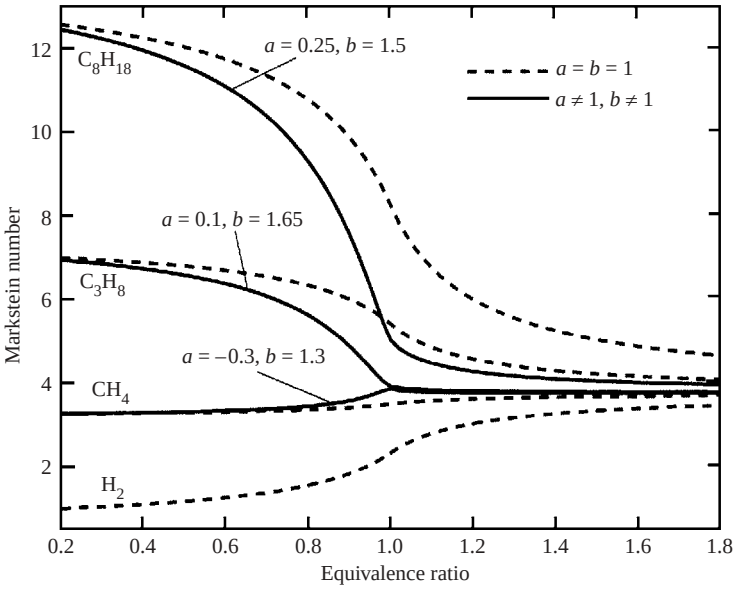

FIGURE 2. The dependence of the Markstein number on equivalence ratio for selected fuel/air mixtures. For hydrocarbon fuels, the dependence is also shown for non-unity reaction orders.

the Markstein number depends explicitly on the mixture's equivalence ratio, as well as on the reaction orders with respect to each of the two reactants. The effective Lewis number (6.12) is expressed as a weighted average of the Lewis numbers of the two reactants. Under exact stoichiometry, since $\mathscr{G}(a, b; 0) = \Gamma(a + b + 1)$, we find that $\mathscr{A} = a/b$ and the effective Lewis number is the mean of the Lewis numbers of the two reactants, $Le_{\text{eff}} = (bLe_E + aLe_D)/(a + b)$. As φ increases, the deficient reactant in the mixture becomes more and more heavily weighted. For conditions sufficiently far from stoichiometry, i.e. $\varphi \to \infty$, the asymptotic relation $\mathscr{G}(a, b, z) \sim \beta^b \Gamma(a + 1)$ implies that $\mathscr{A} \to \infty$, and the effective Lewis number is that of the deficient reactant. When $a = b = 1$, $\mathscr{A} = 1 + \varphi$ and we recover the expression for Le_{eff} that appeared in Bechtold & Matalon (2001). The dependence of the Markstein number on equivalence ratio is shown in figure 2 for selected fuel/air mixtures with $a = b = 1$, and for the hydrocarbon–air mixtures with non-unity values as well based on those suggested by Westbrook & Dryer (1981). The computations are based on the realistic choice $\lambda \sim T^{1/2}$ and, for purpose of comparison, the same values of $\sigma = 6$ and $\beta = 10$ have been chosen for all cases. While there are significant differences at lean conditions with the heavier fuels corresponding to larger values of α, all curves tend to the same limit for rich conditions, being all associated with the binary mass diffusivity of O_2–N_2. In real systems, however, this limit may vary from one mixture to another as a result of variations in β and σ. For the heavy hydrocarbon–air mixtures, an increase in mixture strength from lean to rich results in a decrease in the effective Lewis number and hence a decrease in the Markstein number. For the lighter fuels, such as methane and hydrogen, the Markstein number increases with mixture strength. Finally, non-unity reaction orders, that appear to better correlate experimental data, seem to have a significant effect on the Markstein number, particularly at near-stoichiometric conditions.

The convention used in this paper is to define the flame speed relative to the gas velocity ahead of the flame. Alternatively one could use a definition of flame speed,

and consequently of Markstein number, defined relative to the gas velocity of the burned gas behind the flame. Then, using (6.7) and the jump condition (6.4), the flame speed normalized with respect to the laminar flame speed defined relative to the burned gas is $S_f^{\rm b}/\sigma = 1 - \delta\alpha^{\rm b}K$, with the Markstein number

$$\alpha^{\rm b} = \frac{1}{\sigma-1}\int_1^\sigma \frac{\lambda(x)}{x}\,{\rm d}x + \frac{\beta(Le_{\rm eff}-1)}{2(\sigma-1)}\int_1^\sigma \frac{\lambda(x)}{x}\ln\left(\frac{\sigma-1}{x-1}\right){\rm d}x\,. \tag{6.13}$$

It is important to note that the Markstein number is uniquely defined only in the asymptotic limit considered here, where the whole flame is treated as a hydrodynamic discontinuity that coincides with the reaction sheet and the flame speed is evaluated at this location. In real flames of finite thickness the actual gas speed, and hence S_f, is only known to within an amount proportional to the flame thickness. Thus, the magnitude of the Markstein correction is not uniquely determined. Experimental measurements, on the other hand, are typically taken at a specific reference location inside the flame zone. To make meaningful comparisons between theory and experiments the Markstein number must therefore be adjusted by properly calculating the gas velocity at the chosen reference location, as carried out by Tien & Matalon (1991) and more recently, under more general conditions, by Bechtold & Matalon (2001). Graphs similar to figure 2 were plotted in Bechtold & Matalon (2001) for the adjusted Markstein number, showing good agreement with experimental measurements. Those results also show that the magnitude of the Markstein number decreases as a result of that adjustment and that light fuels may possibly have negative values at lean conditions.

7. Vorticity production

Although the jump in vorticity across the flame front can be easily deduced from equations (6.1)–(6.2) using the jump relations derived above, it is instructive to examine the source of the vorticity production by determining its distribution inside the flame zone. An equation for the vorticity vector $\boldsymbol{\omega} = \nabla\times\boldsymbol{v}$ can be obtained by taking the curl of the momentum equation (2.2) of the form

$$\frac{{\rm D}\boldsymbol{\omega}}{{\rm D}t} + (\boldsymbol{\omega}\cdot\nabla)\,\boldsymbol{v} - (\nabla\cdot\boldsymbol{v})\,\boldsymbol{\omega} = \frac{1}{\rho^2}(\nabla\rho\times\nabla p) + \delta Pr\,\nabla\times\left(\frac{1}{\rho}\nabla\cdot\lambda\boldsymbol{\Sigma}\right). \tag{7.1}$$

In the flame zone this equation simplifies, to leading order, to

$$\frac{\partial\omega_n}{\partial\eta} = 0,$$

$$\frac{\partial}{\partial\eta}\left(\frac{\boldsymbol{\omega}_\perp}{\rho^{(0)}}\right) = -\frac{\partial}{\partial\eta}\left(\frac{\boldsymbol{n}\times\tilde{\nabla}_s p^{(0)}}{\rho^{(0)}}\right) + Pr\,\frac{\partial}{\partial\eta}\left\{\frac{1}{\lambda\rho^{(0)}}\boldsymbol{n}\times\left(\frac{\partial^2\boldsymbol{v}_\perp^{(1)}}{\partial\eta^2} + \frac{\partial\lambda}{\partial\eta}\left(\boldsymbol{w}^{(0)} + \tilde{\nabla}_s u^{(0)}\right)\right)\right\},$$

where $\boldsymbol{\omega} = \boldsymbol{\omega}_\perp\boldsymbol{e}_1 + \omega_n\boldsymbol{n}$. Clearly, the normal component of the vorticity is conserved through the flame. Variations in the transverse components may only result from the baroclinic and viscous diffusion effects, while intensification due to bending and stretching of vortex lines (the second and third terms of (7.1)) are negligible. It is easy to verify from (3.4)–(3.5) that $\boldsymbol{\omega}$ remains continuous at the reaction sheet, so that the solution that matches the vorticity $\boldsymbol{\Omega}$ in the upstream hydrodynamic region, i.e. as

$\eta \to -\infty$, is of the form

$$\omega_n = \Omega_n, \tag{7.2}$$

$$\boldsymbol{\omega}_\perp = \rho^{(0)}\boldsymbol{\Omega}_\perp + \left(\rho^{(0)} - 1\right)\left(\boldsymbol{n} \times \tilde{\nabla}_s p^{(0)}\right) + \frac{Pr}{\lambda}\boldsymbol{n} \times \left\{ \frac{\partial^2 \boldsymbol{v}_\perp^{(1)}}{\partial \eta^2} + \frac{\partial \lambda}{\partial \eta}\left(\boldsymbol{w}^{(0)} + \tilde{\nabla}_s u^{(0)}\right) \right\}, \tag{7.3}$$

where $\boldsymbol{\Omega} = \boldsymbol{\Omega}_\perp + \Omega_n \boldsymbol{n}$ is evaluated at $n = 0^-$. Although the explicit solution for $\boldsymbol{\omega}_\perp$ can be easily obtained, it requires the solution of $\boldsymbol{v}_\perp^{(1)}$, which we have avoided writing down. Nevertheless, by examining the limiting behaviours of (7.3) as $\eta \to \pm\infty$, one immediately finds the jump relation

$$[\![\boldsymbol{\omega}_\perp]\!] = -\frac{\sigma - 1}{\sigma}\boldsymbol{\Omega}_\perp - \frac{\sigma - 1}{\sigma}\left(\boldsymbol{n} \times \tilde{\nabla}_s P^{(0)}\right).$$

While there are variations in vorticity introduced by the gas viscosity, these appear to have no overall effect on the changes across the flame, to leading order. Indeed, from the solution of $\boldsymbol{v}_\perp^{(1)}$ it can be verified that the term multiplying Pr in (7.3) vanishes as $\eta \to -\infty$ and is identically zero for $\eta \geqslant 0$.

To determine the $O(\delta)$ corrections to the vorticity jump, it is not necessary to carry the analysis in the flame zone to higher orders. All that is needed is the jump in derivatives of the velocities and these can be obtained directly by evaluating the momentum equation (6.2) on either side of the flame. We will not write the general result explicitly, because it involves lengthy expressions which can be deduced in any particular situation.

To summarize, the vorticity field in the hydrodynamic regions on either side of the flame is obtained by solving

$$\rho \frac{\mathrm{D}\boldsymbol{\omega}}{\mathrm{D}t} - \rho\,(\boldsymbol{\omega} \cdot \nabla)\,\boldsymbol{v} = \delta Pr \lambda\, \nabla^2 \boldsymbol{\omega} \tag{7.4}$$

subject to the jump condition

$$[\![\boldsymbol{\omega}]\!] = -\frac{\sigma - 1}{\sigma}\left\{\boldsymbol{n} \times (\boldsymbol{\omega} \times \boldsymbol{n}) + \boldsymbol{n} \times \nabla p\right\} + O(\delta). \tag{7.5}$$

Thus, even when the flow of unburned gas is irrotational, vorticity is being generated at the flame and transported downstream, so that the flow of burned gas is, in general, rotational. To leading order, the normal component of vorticity is preserved across the flame front, while the tangential components suffer a jump. The jump in vorticity results from the drop in density of the fluid particles transporting vorticity through the flame zone and from baroclinic production. Changes in vorticity introduced by the gas viscosity are secondary effects appearing only at $O(\delta)$.

For a steady two-dimensional flow the flame sheet is represented by a curve in the plane of motion and the only relevant vorticity component, ω say, is perpendicular to that plane. If use is made of equation (6.2) and of the fact that $u = 1$ ahead of the flame, (7.5) reduces to

$$[\![\omega]\!] = \frac{\sigma - 1}{\sigma}\frac{\partial}{\partial \xi}\left(\frac{v^2}{2}\right). \tag{7.6}$$

The jump in vorticity is seen here to depend on the variation of the velocity component tangential to the flame surface, as previously noted by Uberoi, Kuethe & Menkes (1958).

8. Some simple flame configurations

In this section we consider some simple flame configurations and, in particular, illustrate features related to the effect of variable transport on flame characteristics and to the production and distribution of vorticity inside and across the flame.

8.1. *Plane flame*

When ignited at one end, a plane flame propagates into a quiescent fresh mixture at a unit speed, so that $x = -t$ denotes its position. The burned gas moves away from the front at a speed $u = \sigma - 1$. A plane flame experiences no stretch, and no vorticity is produced in the flame zone. A stability analysis, based on the model presented here, yields an expression for the growth rate ϖ of small disturbances of the form

$$\varpi = \varpi_0 k - \delta\{B_1 + \beta(Le_{\text{eff}} - 1)\, B_2 + PrB_3\}k^2 + \cdots,$$

where k is the wavenumber and the coefficients ϖ_0, B_1, B_2, B_3, given by

$$\varpi_0 = \frac{1}{\sigma + 1}\left(\sqrt{\sigma^3 + \sigma^2 - \sigma} - \sigma\right),$$

$$B_1 = \frac{1}{4}\,\frac{\sigma^3 - \sigma + 2\sigma^2(2\varpi_0 + \sigma + 1)}{\sigma + (\sigma + 1)\varpi_0},$$

$$B_2 = \frac{1}{2}\,\frac{\sigma(\sigma - 1)(\varpi_0 + 1)(\varpi_0 + \sigma)}{\sigma + (\sigma + 1)\varpi_0},$$

$$B_3 = \frac{1}{2}\,\frac{\sigma(\sigma - 1)^2}{\sigma + (\sigma + 1)\varpi_0},$$

are all positive. Such an expression was derived previously by Clavin & Garcia (1983) who, for the purpose of the analysis, wrote the linear version of the jump conditions (6.4)–(6.6). The leading term ϖ_0, which increases with increasing k, is the Darrieus–Landau instability. The three other terms correspond to thermal, mass and viscous diffusion, respectively. When the gas viscosity is assumed constant, the coefficient $B_3 = 0$; see Matalon & Matkowsky (1982) & Pelce & Clavin (1982). In contrast, with the more realistic variable transport one finds that viscosity plays an equal role to other diffusion effects and always has a stabilizing influence. Thermo-diffusive effects have stabilizing influences on the short waves provided Le_{eff} is sufficiently larger than 1 and variable transport properties serve to modify the critical Lewis number.

8.2. *Spherically expanding flame*

We consider an outwardly propagating flame originating from a point source, that propagates into a combustible mixture in an infinite space. Once the flame reaches a size R_0 of several diffusion lengths, i.e. a few millimetres, it can be treated as a hydrodynamic discontinuity. The burned gas trapped by the flame remains motionless, while the flow induced in the fresh mixture corresponds to that of a source originating at the flame front $r = R(t)$. The propagation speed can be easily obtained from the equation for S_f^{b} as

$$\dot{R} = \sigma\left(1 - \delta\alpha^{\text{b}}\frac{2\sigma}{R}\right),$$

where the dot denotes differentiation with respect to t, and $\delta = L_D/R_0$. Note that the flame experiences a stretch rate $K = 2\dot{R}/R \sim 2\sigma/R$ that diminishes in time. Since the flow field remains radial and normal to the front, no vorticity is being created at

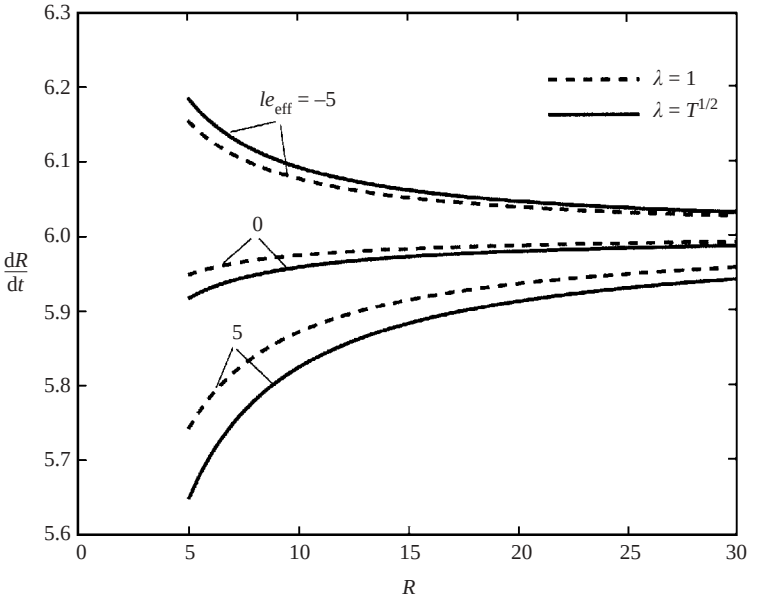

FIGURE 3. Propagation speed of a spherically expanding flame as a function of position. Computed for constant as well as variable transport coefficients, for selected values of the effective Lewis number and with $\delta = 0.01$.

the flame. The irrotational flow in the unburned gas is given by

$$v = (\sigma - 1)\left\{1 - \tfrac{1}{2}\delta\beta(Le_{\text{eff}} - 1)\gamma_2 \frac{2\dot{R}}{R}\right\}\frac{1}{r^2},$$

and, as required, tends to zero as $r \to \infty$ and satisfies the mass conservation (6.4).

In figure 3 we have plotted the propagation speed against the flame position for both cases, $\lambda = 1$ and $\lambda \sim T^{1/2}$. When the effective Lewis number $le_{\text{eff}} > le^*_{\text{eff}}$, with le^*_{eff} slightly negative and corresponding to $\alpha^{\text{b}} = 0$, the propagation speed increases as the flame grows larger. The reverse is true when $le_{\text{eff}} < le^*_{\text{eff}}$. At large radii, the propagation speed eventually approaches the constant speed σ corresponding (in dimensional form) to the laminar flame speed measured with respect to the burned gas. For a given mixture, le^*_{eff} is associated with a critical value of the equivalence ratio that identifies the transition from one behaviour to the other. For example, for propane–air mixtures this critical value is $\phi \approx 1.3$, and the propagation speed increases in time for $\phi < 1.3$ and decreases in time for $\phi > 1.3$, as reported by Addabbo, Bechtold & Matalon (2002), in agreement with the experimental results reported by Strehlow (1984). The graph also shows that, depending on whether le_{eff} is less/greater than le^*_{eff}, the propagation speed is over-/under-estimated by assuming that the transport properties are constant. With the more realistic temperature-dependent transport coefficients, the flame must travel a larger distance to reach the constant laminar speed σ. More important, however, is their influence on flame stability. As shown by Addabo *et al.* (2002), the present model leads to stability results more commensurate with experimental data. In particular, the critical Péclet number that identifies the marginal stability conditions is shifted upwards by nearly 50% and the predictions of cell size correlate better with observations.

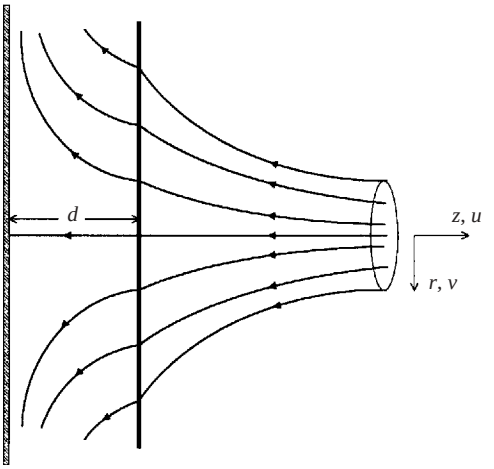

FIGURE 4. Schematic representation of a flame stabilized in a stagnation-point flow. Note the diffraction of the streamlines at the flame front, resulting from the jump in the normal velocity component.

8.3. *Flame stabilized in a stagnation-point flow*

We consider a flame stabilized in a stagnation-point flow of a bluff body of revolution, as illustrated in figure 4. The flame may be treated as a hydrodynamic discontinuity when its stand-off distance, which often is of the order of 1–2 cm, is large compared to the nominal flame thickness L_D. As a result of thermal expansion, the flame displaces the upstream flow a distance a, so that the potential flow ahead is

$$u = -2\epsilon\,(z-a), \qquad v = \epsilon\, r,$$

where ϵ is the strain rate. The displacement a is related to the standoff distance d through the relation $d - a = 1/2\epsilon - \delta\alpha$, obtained from (6.7). The full evaluation of these constants requires first determining the flow field in the burned gas region, as carried out in Eteng, Ludford & Matalon (1986) for the case of constant properties, and is based on solving the vorticity equation (7.4) subject to the jump condition

$$[\![\omega]\!] = -\frac{\sigma-1}{\sigma}\left\{1 - \delta\epsilon\,\frac{2}{\sigma}\left(Pr\lambda_{\rm b} - \tfrac{1}{2}\sigma\, le_{\rm eff}\,\gamma_2\right)\right\}\epsilon^2 r, \tag{8.1}$$

which has been developed here to $O(\delta)$ as outlined above. The rotational flow behind the flame is thus found to be

$$u = -2f(z), \qquad v = r\, f'(z),$$

where

$$f(z) = \frac{\sigma-1}{\sigma}\epsilon^2 z^2 - 2\sqrt{\sigma}\epsilon\, z + \delta\frac{\sigma-1}{\sigma^2}\left(Pr\lambda_{\rm b} - \tfrac{1}{2}\sigma\, le_{\rm eff}\,\gamma_2\right)\epsilon^3 z^2.$$

Finally, the flame stand-off distance is

$$d = \frac{\sigma}{\sigma^{1/2}+1}\epsilon^{-1} - \delta\left\{\gamma_1 + \frac{\sigma^{1/2}-1}{\sigma^{1/2}+1}Pr\lambda_{\rm b} + \frac{\sigma}{\sigma^{1/2}+1}le_{\rm eff}\,\gamma_2\right\}.$$

In figure 5 we show the dependence of d on σ for selected values of $le_{\rm eff}$, calculated with $\lambda = 1$ and $\lambda \sim T^{1/2}$. With realistic transport properties the flame stand-off distance decreases as the Lewis number decreases.

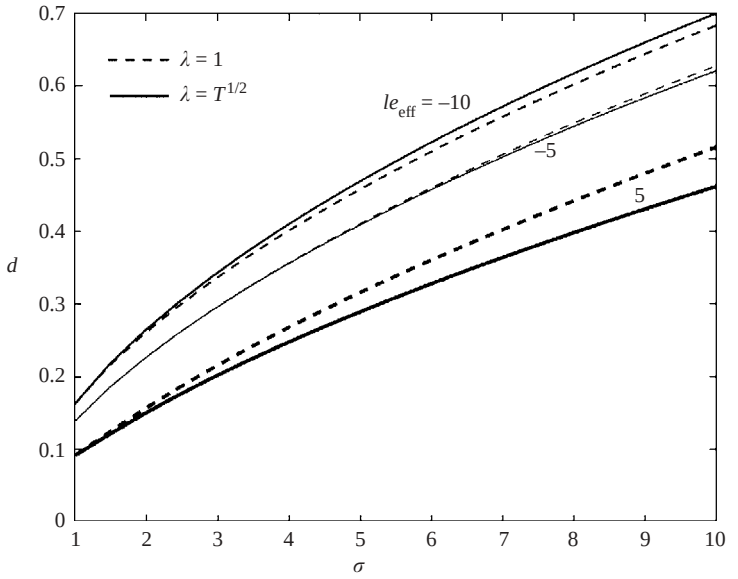

FIGURE 5. The stand-off distance d of a flame in a stagnation-point flow as a function of the thermal expansion parameter σ for selected values of the reduced Lewis number le_{eff}; calculated with $\delta = 0.01$.

It is instructive to examine the primary variations in vorticity throughout the flame which led to the production (8.1). From (7.3) the vorticity distribution, to leading order, is given by

$$\omega = \begin{cases} \left(\dfrac{(\sigma-1)\mathrm{e}^{\eta}}{1+(\sigma-1)\mathrm{e}^{\eta}} + \dfrac{\sigma-1}{\sigma} Pr\, g(\eta) \right) \epsilon^2 r, & \eta < 0 \\ \dfrac{\sigma-1}{\sigma}\, \epsilon^2 r, & \eta > 0, \end{cases} \tag{8.2}$$

where

$$g(\eta) = \frac{\sigma\, \mathrm{e}^{\eta}}{1+(\sigma-1)\mathrm{e}^{\eta}} + \frac{\lambda_b}{\lambda(\eta)} \mathrm{e}^{\eta/Pr} + \frac{Pr}{\lambda(\eta)} \int_{\eta}^{0} \frac{\sigma\, \mathrm{e}^{\eta'}\, \lambda(\eta')}{1+(\sigma-1)\mathrm{e}^{\eta'}}\, \mathrm{e}^{(\eta-\eta')/Pr}\, \mathrm{d}\eta'.$$

Note that the vorticity production occurs in the preheat zone. The first term represents the baroclinic production and the second term the effects due to the gas viscosity. As noted earlier, the latter does not contribute to the overall jump across the flame and indeed $g(0) = 0$ and $g(\eta) \to 0$ as $\eta \to -\infty$. In figure 6 the vorticity distribution throughout the flame zone is plotted at several radial distances r and the separate contributions are illustrated for the case $r = 5$.

8.4. *Bunsen burner flame*

We consider now the Bunsen burner flame. The flow of unburned gas issuing from the burner of width $2a$ is assumed to be a Poiseuille flow, as shown in figure 7. The flame can be treated as a surface of discontinuity since typically $a \gg L_D$. Using a as a unit of length and the laminar flame speed as a unit of speed, the gas velocity ahead of the flame is given by $\boldsymbol{v} = u(y)\boldsymbol{i}$ where $u = U(1-y^2)$ with U the (dimensionless)

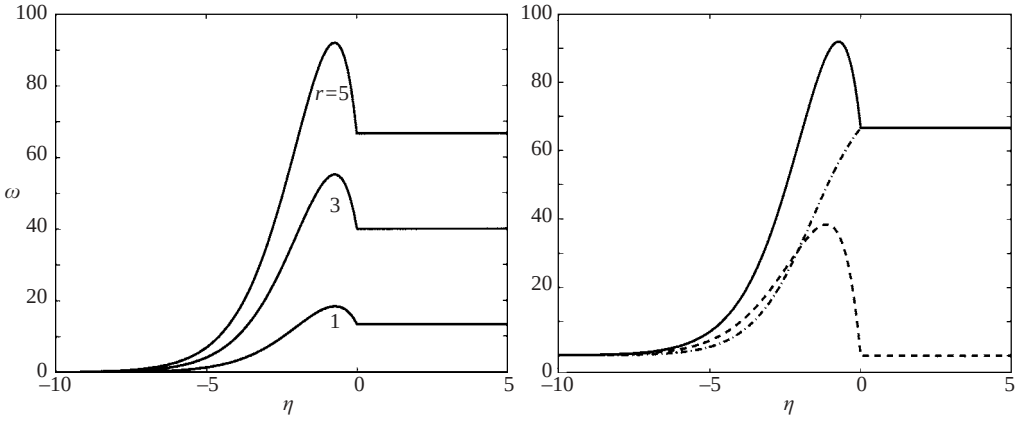

FIGURE 6. (*a*) Vorticity variations across the flame zone at several radial distances. (*b*) The separate contributions of baroclinic effect (dot-dashed curve) and gas viscosity (dashed curve) for $r = 5$; the latter has a zero net contribution to the overall jump across the flame.

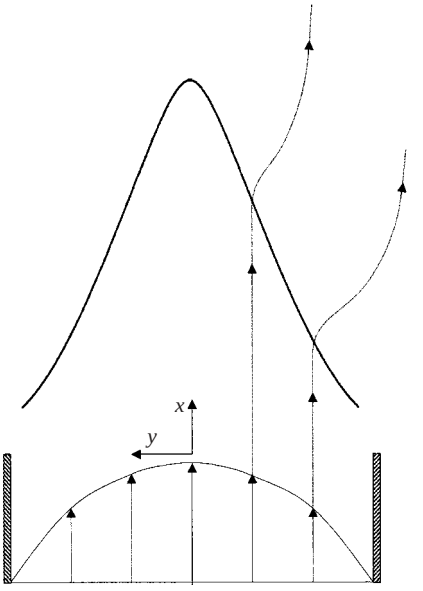

FIGURE 7. Bunsen burner flame and representative streamlines showing their refraction across the flame front; the front was calculated based the equation $F(x, y) = 0$ with a prescribed Poiseuille flow.

centreline velocity and y the transverse coordinate. If the flame front is described by $F(x, y) \equiv x - f(y) = 0$, and ψ denotes the slope $\mathrm{d}f/\mathrm{d}y$, unit vectors normal and tangential to the flame front are given by

$$\boldsymbol{n} = \frac{\boldsymbol{i} - \psi\,\boldsymbol{j}}{(1+\psi^2)^{1/2}}, \qquad \boldsymbol{e} = \frac{\psi\,\boldsymbol{i} + \boldsymbol{j}}{(1+\psi^2)^{1/2}},$$

with $\boldsymbol{i}$, $\boldsymbol{j}$ unit vectors in the x, y-directions, respectively. Under steady conditions, the flame speed is just the normal component of the gas velocity at the flame front,

namely $S_f = u(y)/(1+\psi^2)^{1/2}$. The stretch rate is given by

$$K = \frac{\psi}{1+\psi^2}\frac{\mathrm{d}u}{\mathrm{d}y} + \frac{u}{(1+\psi^2)^{1/2}}\frac{1}{(1+\psi^2)^{3/2}}\frac{\mathrm{d}\psi}{\mathrm{d}y}, \tag{8.3}$$

where the first term, equal to K_s, is due to strain and the second, equal to $S_f\kappa$, is due to curvature. Since, to leading order, $(1+\psi^2)^{1/2} \sim u$, the flame stretch $K \sim (1+\psi^2)^{-1/2}\,\psi'$ (where a prime denotes differentiation) and, correct to $O(\delta)$, the flame speed relation (6.7) reduces to

$$\sqrt{(1+\psi^2)} - U(1-y^2) = \delta\alpha\frac{\mathrm{d}\psi}{\mathrm{d}y}. \tag{8.4}$$

The solution

$$\psi \sim \mp U\left[\left(\frac{U+1}{U}-y^2\right)\left(\frac{U-1}{U}-y^2\right)\right]^{1/2} - 2\delta\alpha\frac{U^3(1-y^2)^2\,y}{U^2(1-y^2)^2-1} \tag{8.5}$$

is clearly limited to $|y| < [(U-1)/U]^{1/2}$. The flame shape is given by $x = H + \int_0^y \psi(\bar{y})\,\mathrm{d}\bar{y}$ where the integral can be expressed in terms of Elliptic functions and H is the flame height. Note that ψ' is always positive implying that the flame is everywhere concave-up. As $U \to \infty$, the flame extends to $y = \pm 1$ and is given by $x \sim H \mp U(y - y^3/3) - \delta\alpha U y^2$.

The solution (8.5) fails at the tip $y = 0$, because of a discontinuity in slopes, and at the two end points $y = \pm[(U-1)/U]^{1/2}$, because the slopes become infinite there. A complete description of the hydrodynamics near the flame tip and edges is quite complex and is beyond the scope of this work. No general description has been given, although a relevant discussion of slender flame tips was given by Buckmaster & Crowley (1983). Insight can be obtained if one adopts the flame speed equation (6.7) as an approximation, which states that the burning velocity is increased significantly in the region of strong curvature. Then, near the tip, $y = \delta\eta$, the gas speed is nearly constant $\sim U$, the stretch rate $K \sim S_f\kappa$ is primarily due to curvature (with no contribution from the strain rate), and

$$\frac{U}{(1+\psi^2)^{1/2}} = 1 - \frac{\alpha U}{(1+\psi^2)^2}\frac{\mathrm{d}\psi}{\mathrm{d}\eta}.$$

A direct integration yields

$$\alpha^{-1}\eta = -\frac{\psi}{\sqrt{1+\psi^2}} - \frac{1}{U}\tan^{-1}\psi - \frac{2}{U\sqrt{U^2-1}}\tanh^{-1}\left\{\sqrt{\frac{U+1}{U-1}}\,\frac{\sqrt{1+\psi^2}-1}{\psi}\right\},$$

which vanishes at $\eta = 0$ and matches with (8.5) as $\eta \to \pm\infty$, thus connecting smoothly the discontinuity in slopes observed on the larger scale y. Note that, as α decreases, the variations in ψ occur only in a narrower and narrower region near the tip, and that the solution is no longer valid when $\alpha < 0$. This may be related to the phenomenon of open tips (cf. Lewis & von Elbe 1987), observed in lean hydrogen–air or rich propane–air mixtures for example, namely when the effective Lewis number is sufficiently less than 1.

Near the edges, we write

$$y = \mp\sqrt{\frac{U-1}{U}} \pm 2\delta^{2/3}\eta, \qquad \psi = \mp\delta^{1/3}\,\Psi,$$

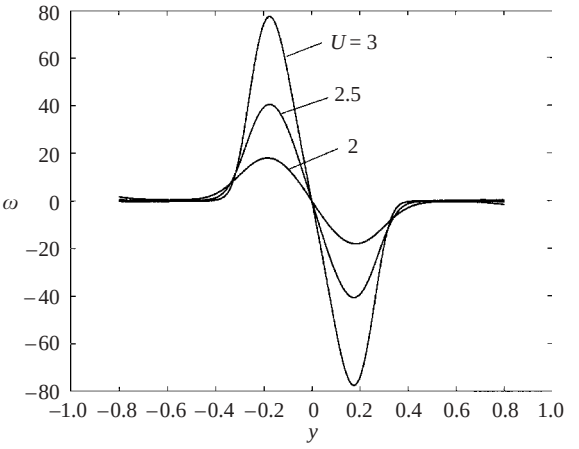

FIGURE 8. Vorticity generated at the flame front, calculated with $\delta = 0.05$, $\sigma = 6$ and $le_{\text{eff}} = 4$.

to obtain from (6.7) the equation

$$\alpha \frac{\mathrm{d}\Psi}{\mathrm{d}\eta} = -\Psi^2 + \alpha^2 N^{-3}\,\eta,$$

with $N \equiv \alpha^{2/3}/2[U(U-1)]^{1/6}$, where again, stretch is primarily due to curvature. This is a Ricatti equation which reduces to the linear Airy equation $\Phi'' - N^{-3}\,\eta\Phi = 0$ when applying the substitution $\Psi = \Phi'/\Phi$, with solutions of the form $\Phi = C_1 \mathrm{Ai}(N\eta) + C_2\,\mathrm{Bi}(N\eta)$. The solution that matches (8.5) as $\eta \to +\infty$ and extends the slope smoothly to small values of η, is

$$\psi = \delta^{1/3}\alpha N^{-2}\frac{\mathrm{Ai}'(N\eta)}{\mathrm{Ai}(N\eta)}.$$

In reality, this region is affected by the presence of the burner, with the flame stabilized by the heat conducted back to the rim.

The solution can be more simply illustrated if the flame speed is integrated numerically with K given by (8.3), while retaining δ small. The solution calculated with $\delta = 0.05$ is shown in figure 7. Note the concavity of the flame surface which indicates that the flame is generally stretched ($K > 0$) except near the tip, where it is compressed ($K < 0$). Also shown is the refraction of streamlines crossing the flame front. Since the normal velocity component increases six- to seven-fold while the velocity components tangential to the flame remain unchanged (to leading order), streamlines generally rotate towards the direction of the normal.

The vorticity generated at the flame can be calculated to leading order from (7.6) with the $O(\delta)$ correction following the scheme sketched above. In figure 8 we show the vorticity generated behind the flame for different values of U. We see that large vorticity is being generated at the highly curved region of the flame near the tip. Along the axis of the burner, the streamline is parallel to the axis. Adjacent streamlines, however, are strongly rotated towards the normal. When moving further away from the axis, the vorticity generated at the front reduces and thus causes a relatively smaller change in the streamline rotation, as illustrated in figure 9. The behaviour shown in figure 8 changes significantly near the extremity of the tip when increasing U or decreasing the Lewis number. It is found that a pair of counter-rotating vortices

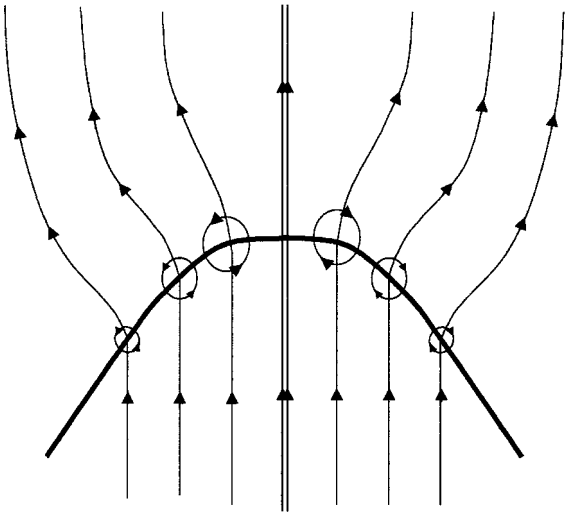

FIGURE 9. Sketch of streamlines rotated by the vorticity generated at the flame, in the region near the tip.

is then generated and this may possibly correspond to the opening of the tip discussed earlier.

9. Conclusions

Premixed flames have often been treated as propagating fronts separating the cold fresh mixture from the hot burned products. As such the mathematical problem reduces to a fluid dynamic problem involving a free boundary, and one is left to identify the law of propagation, which is commonly expressed as an equation for the flame speed. In the early theories and in the more current numerical simulations based on the so-called G-equation, the propagation law is specified. The objective of this work has been to formulate a hydrodynamic model that treats the flame as a front and systematically derive an equation for the flame speed by resolving, on the relatively smaller diffusion scale, the internal structure of the flame. The formulation also consists of modified jump conditions in the form of corrected Rankine–Hugoniot relations that need to be satisfied across the flame front. The flame speed and jump conditions mimic the diffusion processes occurring in the flame zone and depend explicitly on all the relevant physico-chemical parameters. The present theory extends the earlier work of Matalon & Matkowsky (1982) by (i) adopting an intrinsic coordinate system and thus presenting a formulation in coordinate-free form, (ii) using a two-reactant model and thus extending the results to mixtures that span from lean to rich conditions, (iii) using arbitrary reaction orders and thus allowing a global representation of more complex reaction schemes, and (iv) allowing temperature-dependent transport coefficients and thus improving the quantitative predictions of the model.

The multi-scale analysis presented in this paper assumes that the flame is only affected by disturbances evolving on the time scale associated with the external flow. Consequently the flame structure that includes the preheat and the reaction zones remains quasi-steady and, being thin, also quasi-planar. Our model captures the well-known Darrieus–Landau instability, clarifies the influence of thermal, mass and

viscous diffusion and identifies the mechanism of vorticity production, as illustrated by some simple flame configurations. However, it does not capture another well-known form of flame instability associated with oscillations that has been understood well in constant-density flows. To do so requires incorporating the time-dependent dynamics associated with the diffusive effects that occur on a scale comparable with the preheat zone in the analysis. While this has not been done in general, the high-frequency analysis of Joulin (1994) and Clavin & Joulin (1997) is a step in that direction.

This work has been partially supported by the National Science Foundation under grants DMS-0072588 and CTS-0074320 and by NASA's Microgravity Combustion Program under grant NAG3-2511.

Appendix A. Flame stretch

A surface element A made up of points on the flame surface that travel along it with a velocity $\boldsymbol{v}_\perp$ is, in general, deformed by the motion so that A varies with time. A measure of this deformation is the proportionate rate of change of the surface element, i.e. $K = A^{-1}\mathrm{d}A/\mathrm{d}t$, referred to as flame stretch (cf. Williams 1985; Buckmaster & Ludford 1982). We note that $\mathrm{d}/\mathrm{d}t$ here is not a material derivative since the surface element is not made up of the same fluid particles. The definition clearly requires the identification of a flame surface and is, therefore, meaningful only in the asymptotic sense considered here where it is unambiguously chosen as the surface that results when $\delta \to 0$.

Flame stretch characterizes the distortion of the flame surface resulting from its propagation, with speed V_f, and from the underlying fluid motion along the surface, with velocity $\boldsymbol{v}_\perp$. It has units of s^{-1} and its dimensionless form, often referred to as the Karlovitz number, is thus obtained after multiplication by the factor $\delta L_D/S_L$. A general expression in coordinate-free form was first given by Matalon (1983) as

$$K = V_f\, \nabla\cdot\boldsymbol{n} - \boldsymbol{n}\cdot\nabla\times(\boldsymbol{v}\times\boldsymbol{n}). \tag{A 1}$$

Expanding the last term on the right, this expression can be rewritten in the form

$$K = -S_f\ \nabla\cdot\boldsymbol{n} - \boldsymbol{n}\cdot\boldsymbol{E}\cdot\boldsymbol{n}$$

identifying the separate contributions due to curvature $\kappa = -\nabla\cdot\boldsymbol{n}$ and strain $K_s = -\boldsymbol{n}\cdot\boldsymbol{E}\cdot\boldsymbol{n}$, namely $K = S_f\,\kappa + K_s$. Note that only when the flame can be treated as a hydrodynamic discontinuity with the flame speed equal to 1 to leading order, is the total stretch $K \sim \kappa + K_s$ the sum of curvature and strain.

When intrinsic surface coordinates ξ_1, ξ_2 are used, (A 1) takes the form

$$K = -V_f\ \kappa + \frac{1}{a_1 a_2}\left\{\frac{\partial(a_2 v_1)}{\partial\xi_1} + \frac{\partial(a_1 v_2)}{\partial\xi_2}\right\}$$

or, noting that on the flame surface $l_1 = a_1$ and $l_2 = a_2$, the form $K = -V_f\,\kappa + \nabla_s\cdot\boldsymbol{v}_\perp$.

Appendix B. Curvilinear coordinates

Let $\boldsymbol{r} = \boldsymbol{r}(\boldsymbol{x}, t)$ be the vector position of a point P in space, measured at time t, with respect to a fixed coordinate system, where $\boldsymbol{x} = (x_1, x_2, x_3)$. Let the reaction sheet surface, $F(\boldsymbol{x}, t) = 0$, be parameterized by the two surface coordinates (ξ_1, ξ_2) aligned with the principal directions of curvature at each point of the surface. The reaction

sheet, at any instant t, is thus described by $\boldsymbol{r} = \boldsymbol{r}_f(\xi_1, \xi_2, t)$. The position of the point P in space may be expressed in terms of the distance n from the reaction sheet and the position vector $\boldsymbol{r}_f$ of the projection of P on the surface (see figure 1), namely

$$\boldsymbol{r} = \boldsymbol{r}_f(\xi_1, \xi_2, t) + n\,\boldsymbol{n}(\xi_1, \xi_2, t), \tag{B 1}$$

where $\boldsymbol{n}$ denotes a unit normal to the surface and, for definiteness, is considered to point in the direction of the burned gas. Let $\boldsymbol{e}_1$ and $\boldsymbol{e}_2$ denote unit vectors tangential to the parametric curves $\xi_2 = \text{const.}$ and $\xi_1 = \text{const.}$, respectively, then

$$\boldsymbol{e}_1 = \frac{1}{a_1}\frac{\partial \boldsymbol{r}_f}{\partial \xi_1}, \qquad \boldsymbol{e}_2 = \frac{1}{a_2}\frac{\partial \boldsymbol{r}_f}{\partial \xi_2}, \tag{B 2}$$

with $a_i = |\partial \boldsymbol{r}_f/\partial \xi_i|$. The three vectors $\boldsymbol{e}_1, \boldsymbol{e}_2, \boldsymbol{n}$ thus form an orthogonal triad of unit vectors and (ξ_1, ξ_2, n) may be taken as curvilinear coordinates of P in these three directions, respectively.

Relation (B 1) serves as the transformation that relates the rectangular coordinates (x_1, x_2, x_3) to the new coordinates, and can be inverted to express ξ_1, ξ_2, n in terms of x_1, x_2, x_3, assuming that the correspondence is unique. Standard results from differential geometry (e.g. Weatherburn 1961) provide the scale factors

$$l_1 = a_1(1 - n\kappa_1), \qquad l_2 = a_2(1 - n\kappa_2), \qquad l_3 = 1, \tag{B 3}$$

used in the computation of the vector differential operators; here κ_1 and κ_2 are the principal curvatures in the ξ_1- and ξ_2-directions, respectively, so that $\kappa = \kappa_1 + \kappa_2$ is twice the mean curvature of the surface. The scale factors of curvilinear coordinates in general are not independent but must satisfy six compatibility differential relations (Lamé 1859), also known as Lamé's relations; cf. Struik (1961) and Weatherburn (1961). In the present case, since $l_3 = 1$, they reduce to the three relations

$$\left.\begin{aligned} &\frac{\partial}{\partial \xi_2}(a_1\kappa_1) = \kappa_2 \frac{\partial a_1}{\partial \xi_2}, \\ &\frac{\partial}{\partial \xi_1}(a_2\kappa_2) = \kappa_1 \frac{\partial a_2}{\partial \xi_1}, \\ &\frac{\partial}{\partial \xi_1}\left(\frac{1}{a_1}\frac{\partial a_2}{\partial \xi_1}\right) + \frac{\partial}{\partial \xi_2}\left(\frac{1}{a_2}\frac{\partial a_1}{\partial \xi_2}\right) + a_1 a_2\,\kappa_1\kappa_2 = 0. \end{aligned}\right\} \tag{B 4}$$

We note that in two dimensions, when the surface reduces to a curve and $a_2 = 0$, one may take $a_1 = 1$ without loss of generality, which amounts to ξ_1 being a measure of the arclength; otherwise a_1 and a_2 cannot be both taken equal to 1 except for developable surfaces.

Vector operators in the curvilinear coordinates can be found in textbooks and will not be repeated here. We find it convenient, however, to introduce the surface gradient

$$\nabla_s = \boldsymbol{e}_1 \frac{1}{l_1}\frac{\partial}{\partial \xi_1} + \boldsymbol{e}_2 \frac{1}{l_2}\frac{\partial}{\partial \xi_2},$$

so that $\nabla = \nabla_s + \boldsymbol{n}\partial/\partial n$. Expressions for the rate of strain tensor in the curvilinear coordinates can be found in Goldstein (1938), for example. The only complication arises from the fact that the curvilinear coordinates (ξ_1, ξ_2, n) are attached to a moving surface. If the time variable in the moving frame is also denoted by t (to avoid unnecessary additional notation), time derivatives in the moving frame are

related to those in a fixed system via

$$\frac{\partial}{\partial t} \mapsto \frac{\partial}{\partial t} + \frac{\partial \xi_1}{\partial t}\frac{\partial}{\partial \xi_1} + \frac{\partial \xi_2}{\partial t}\frac{\partial}{\partial \xi_2} + \frac{\partial n}{\partial t}\frac{\partial}{\partial n}$$
$$= \frac{\partial}{\partial t} + \boldsymbol{q}\cdot\nabla_s - V_f\frac{\partial}{\partial n}, \tag{B 5}$$

where $V_f = -\partial n/\partial t$ and $\boldsymbol{q} = q_1\boldsymbol{e}_1 + q_2\boldsymbol{e}_2$ with $q_i = l_i\,\partial\xi_i/\partial t$ for $i = 1, 2$. Here V_f represents the velocity of the surface back along its normal and q_i is the time rate of change of an arclength along the coordinate curves ξ_i. Time derivatives of a scalar in the moving frame are easily expressed by means of the transformation (B 5). Its application to a vector, however, necessitates finding expressions for the derivatives of the unit vectors that can be appropriately decomposed in the $\boldsymbol{e}_1$-, $\boldsymbol{e}_2$-, $\boldsymbol{n}$-directions.

Spatial derivatives of the unit vectors

Spatial derivatives of the units vectors can be found in standard textbooks (e.g. Batchelor 1967; Weatherburn 1961) where

$$\left.\begin{array}{lll} \dfrac{\partial \boldsymbol{e}_1}{\partial \xi_1} = -\dfrac{1}{a_2}\dfrac{\partial a_1}{\partial \xi_2}\boldsymbol{e}_2 + a_1\kappa_1\boldsymbol{n} & \dfrac{\partial \boldsymbol{e}_1}{\partial \xi_2} = \dfrac{1}{a_1}\dfrac{\partial a_2}{\partial \xi_1}\boldsymbol{e}_2 & \dfrac{\partial \boldsymbol{e}_1}{\partial n} = 0, \\ \dfrac{\partial \boldsymbol{e}_2}{\partial \xi_2} = -\dfrac{1}{a_1}\dfrac{\partial a_2}{\partial \xi_1}\boldsymbol{e}_1 + a_2\kappa_2\boldsymbol{n} & \dfrac{\partial \boldsymbol{e}_2}{\partial \xi_1} = \dfrac{1}{a_2}\dfrac{\partial a_1}{\partial \xi_2}\boldsymbol{e}_1 & \dfrac{\partial \boldsymbol{e}_2}{\partial n} = 0, \\ \dfrac{\partial \boldsymbol{n}}{\partial \xi_1} = -a_1\kappa_1\boldsymbol{e}_1 & \dfrac{\partial \boldsymbol{n}}{\partial \xi_2} = -a_2\kappa_2\boldsymbol{e}_2 & \dfrac{\partial \boldsymbol{n}}{\partial n} = 0. \end{array}\right\} \tag{B 6}$$

Time derivative of the unit vectors

We consider a fixed point in space noting that, since its coordinates in the rectangular frame are fixed in time, $\mathrm{d}\boldsymbol{r}/\mathrm{d}t = 0$. Differentiating (B 1) yields

$$\frac{\partial \boldsymbol{r}_f}{\partial t} + \frac{\partial \xi_1}{\partial t}\frac{\partial \boldsymbol{r}_f}{\partial \xi_1} + \frac{\partial \xi_2}{\partial t}\frac{\partial \boldsymbol{r}_f}{\partial \xi_2} + \frac{\partial n}{\partial t}\boldsymbol{n} + n\left\{\frac{\partial \boldsymbol{n}}{\partial t} + \frac{q_1}{l_1}\frac{\partial \boldsymbol{n}}{\partial \xi_1} + \frac{q_2}{l_2}\frac{\partial \boldsymbol{n}}{\partial \xi_2}\right\} = 0$$

or, equivalently

$$\frac{\partial \boldsymbol{r}_f}{\partial t} + \frac{a_1 q_1}{l_1}\boldsymbol{e}_1 + \frac{a_2 q_2}{l_2}\boldsymbol{e}_2 - V_f\boldsymbol{n} + n\left\{\frac{\partial \boldsymbol{n}}{\partial t} + \frac{q_1}{l_1}\frac{\partial \boldsymbol{n}}{\partial \xi_1} + \frac{q_2}{l_2}\frac{\partial \boldsymbol{n}}{\partial \xi_2}\right\} = 0. \tag{B 7}$$

Since $\boldsymbol{e}_1, \boldsymbol{e}_2, \boldsymbol{n}$ are defined on the surface it is sufficient, for the determination of the time rate of change of the unit vectors, to evaluate this last expression at $n = 0$. Consequently, we find that

$$\frac{\partial \boldsymbol{r}_f}{\partial t} + q_1^o\boldsymbol{e}_1 + q_2^o\boldsymbol{e}_2 - V_f\,\boldsymbol{n} = \boldsymbol{0}, \tag{B 8}$$

where the superscript o in q_i^o indicates that q_i has been evaluated at $n = 0$. We note parenthetically that, by subtracting the last two expressions,

$$\left(\frac{a_1}{l_1}q_1 - q_1^o\right)\boldsymbol{e}_1 + \left(\frac{a_2}{l_2}q_2 - q_2^o\right)\boldsymbol{e}_2 + n\left\{\frac{\partial \boldsymbol{n}}{\partial t} + \frac{q_1}{l_1}\frac{\partial \boldsymbol{n}}{\partial \xi_1} + \frac{q_2}{l_2}\frac{\partial \boldsymbol{n}}{\partial \xi_2}\right\} = 0, \tag{B 9}$$

which can be verified later, for consistency.

Differentiating (B 8) with respect to ξ_i, using that

$$\frac{\partial^2 \boldsymbol{r}_f}{\partial \xi_i \partial t} = \frac{\partial^2 \boldsymbol{r}_f}{\partial t \partial \xi_i} = \frac{\partial}{\partial t}(a_i \boldsymbol{e}_i) = \frac{\partial a_i}{\partial t}\boldsymbol{e}_i + a_i \frac{\partial \boldsymbol{e}_i}{\partial t},$$

yields

$$\frac{\partial a_i}{\partial t}\boldsymbol{e}_i + a_i \frac{\partial \boldsymbol{e}_i}{\partial t} + \frac{\partial q_1^o}{\partial \xi_i}\boldsymbol{e}_1 + \frac{\partial q_2^o}{\partial \xi_i}\boldsymbol{e}_2 + q_1^o \frac{\partial \boldsymbol{e}_1}{\partial \xi_i} + q_2^o \frac{\partial \boldsymbol{e}_2}{\partial \xi_i} - \frac{\partial V_f}{\partial \xi_i}\boldsymbol{n} - V_f \frac{\partial \boldsymbol{n}}{\partial \xi_i} = 0,$$

for $i = 1, 2$. When these two equations are projected onto the three directions $\boldsymbol{e}_1$, $\boldsymbol{e}_2$, $\boldsymbol{n}$, and use is made of (B 6), one finds the six relations

$$\left.\begin{aligned}
&\frac{\partial q_1^o}{\partial \xi_1} + \frac{\partial a_1}{\partial t} + \frac{q_2^o}{a_2}\frac{\partial a_1}{\partial \xi_2} + a_1\kappa_1 V_f = 0, \quad && \frac{\partial q_2^o}{\partial \xi_2} + \frac{\partial a_2}{\partial t} + \frac{q_1^o}{a_1}\frac{\partial a_2}{\partial \xi_1} + a_2\kappa_2 V_f = 0,\\
&\frac{\partial \boldsymbol{e}_1}{\partial t}\cdot\boldsymbol{e}_2 - \frac{q_1^o}{a_1 a_2}\frac{\partial a_1}{\partial \xi_2} + \frac{1}{a_1}\frac{\partial q_2^o}{\partial \xi_1} = 0, && \frac{\partial \boldsymbol{e}_2}{\partial t}\cdot\boldsymbol{e}_1 - \frac{q_2^o}{a_1 a_2}\frac{\partial a_2}{\partial \xi_1} + \frac{1}{a_2}\frac{\partial q_1^o}{\partial \xi_2} = 0,\\
&\frac{\partial \boldsymbol{e}_1}{\partial t}\cdot\boldsymbol{n} + \kappa_1 q_1^o - \frac{1}{a_1}\frac{\partial V_f}{\partial \xi_1} = 0, && \frac{\partial \boldsymbol{e}_2}{\partial t}\cdot\boldsymbol{n} + \kappa_2 q_2^o - \frac{1}{a_2}\frac{\partial V_f}{\partial \xi_2} = 0.
\end{aligned}\right\} \tag{B 10}$$

We note that in two dimensions, retaining only $i = 1$ and taking without loss of generality $a_1 = 1$, these relations (with the index 1 removed) simplify to

$$\frac{\partial q^o}{\partial \xi} + \kappa V_f = 0, \qquad \frac{\partial \boldsymbol{e}}{\partial t}\cdot\boldsymbol{n} + \kappa q^o - \frac{\partial V_f}{\partial \xi} = 0\,,$$

which were derived by Yao & Stewart (1996) and used to obtain a differential equation for the rate of change of the orientation of the normal. A simple manipulation of equations (B 10) yields the desired expressions:

$$\left.\begin{aligned}
\frac{\partial \boldsymbol{e}_1}{\partial t} &= \frac{1}{a_1}\left\{\frac{q_1^o}{a_2}\frac{\partial a_1}{\partial \xi_2} - \frac{\partial q_2^o}{\partial \xi_1}\right\}\boldsymbol{e}_2 + \left\{\frac{1}{a_1}\frac{\partial V_f}{\partial \xi_1} - \kappa_1 q_1^o\right\}\boldsymbol{n},\\
\frac{\partial \boldsymbol{e}_2}{\partial t} &= \frac{1}{a_2}\left\{\frac{q_2^o}{a_1}\frac{\partial a_2}{\partial \xi_1} - \frac{\partial q_1^o}{\partial \xi_2}\right\}\boldsymbol{e}_1 + \left\{\frac{1}{a_2}\frac{\partial V_f}{\partial \xi_2} - \kappa_2 q_2^o\right\}\boldsymbol{n},\\
\frac{\partial \boldsymbol{n}}{\partial t} &= \left\{\kappa_1 q_1^o - \frac{1}{a_1}\frac{\partial V_f}{\partial \xi_1}\right\}\boldsymbol{e}_1 + \left\{\kappa_2 q_2^o - \frac{1}{a_2}\frac{\partial V_f}{\partial \xi_2}\right\}\boldsymbol{e}_2.
\end{aligned}\right\} \tag{B 11}$$

For a complete determination of the transformation (B 5), we proceed to derive an expression for the vector $\boldsymbol{q}$. Differentiating (B 7) with respect to n we find, after collecting terms in the $\boldsymbol{e}_1$-, $\boldsymbol{e}_2$-directions respectively, the two relations

$$\frac{\partial q_1}{\partial n} = \frac{1}{a_1}\frac{\partial V_f}{\partial \xi_1} - \kappa_1 q_1^o\,, \qquad \frac{\partial q_2}{\partial n} = \frac{1}{a_2}\frac{\partial V_f}{\partial \xi_2} - \kappa_2 q_2^o, \tag{B 12}$$

which can be recast in a vector form, as

$$\frac{\partial \boldsymbol{q}}{\partial n} = -\frac{\partial \boldsymbol{n}}{\partial t}. \tag{B 13}$$

A direct integration yields

$$q_1 = q_1^o + \left(\frac{1}{a_1}\frac{\partial V_f}{\partial \xi_1} - \kappa_1 q_1^o\right) n, \qquad q_2 = q_2^o + \left(\frac{1}{a_2}\frac{\partial V_f}{\partial \xi_2} - \kappa_2 q_2^o\right) n. \tag{B 14}$$

At this point it can be verified that the condition (B 9) is indeed satisfied.

Material derivatives

As noted earlier, applying the transformation (B 5) to a scalar is straightforward. Thus, with the velocity field expressed as $\boldsymbol{v} = u\,\boldsymbol{n} + \boldsymbol{v}_\perp$, the convective derivative for a scalar ϕ in the moving frame is obtained from

$$\frac{\mathrm{D}\phi}{\mathrm{D}t} \mapsto \frac{\partial\phi}{\partial t} + (\boldsymbol{v}_\perp + \boldsymbol{q})\cdot\nabla_s\phi + (u - V_f)\frac{\partial\phi}{\partial n}.$$

For a vector field, however,

$$\begin{aligned}
\frac{\partial \boldsymbol{F}}{\partial t} &\mapsto \frac{\partial \boldsymbol{F}}{\partial t} + (\boldsymbol{q}\cdot\nabla_s)\boldsymbol{F} - V_f\frac{\partial \boldsymbol{F}}{\partial n} \\
&= \sum_{i=1}^{2}\left\{\frac{\partial F_i}{\partial t} + \boldsymbol{q}\cdot\nabla_s F_i - V_f\frac{\partial F_i}{\partial n}\right\}\boldsymbol{e}_i + \left\{\frac{\partial F_3}{\partial t} + \boldsymbol{q}\cdot\nabla_s F_3 - V_f\frac{\partial F_3}{\partial n}\right\}\boldsymbol{n} \\
&\quad + F_1\left\{\frac{\partial \boldsymbol{e}_1}{\partial t} + \frac{q_1}{l_1}\frac{\partial \boldsymbol{e}_1}{\partial \xi_1} + \frac{q_2}{l_2}\frac{\partial \boldsymbol{e}_1}{\partial \xi_2} - V_f\frac{\partial \boldsymbol{e}_1}{\partial n}\right\} \\
&\quad + F_2\left\{\frac{\partial \boldsymbol{e}_2}{\partial t} + \frac{q_1}{l_1}\frac{\partial \boldsymbol{e}_2}{\partial \xi_1} + \frac{q_2}{l_2}\frac{\partial \boldsymbol{e}_2}{\partial \xi_2} - V_f\frac{\partial \boldsymbol{e}_2}{\partial n}\right\} \\
&\quad + F_3\left\{\frac{\partial \boldsymbol{n}}{\partial t} + \frac{q_1}{l_1}\frac{\partial \boldsymbol{n}}{\partial \xi_1} + \frac{q_2}{l_2}\frac{\partial \boldsymbol{n}}{\partial \xi_2}\right\},
\end{aligned} \tag{B 15}$$

where we need to use expressions (B 6) and (B 11) for the spatial and time derivatives of the unit vectors, in order to decompose the last three bracketed terms in the $\boldsymbol{e}_1$-, $\boldsymbol{e}_2$-, $\boldsymbol{n}$-directions appropriately. The algebra in simplifying these expressions is quite tedious and is therefore presented for only one of these three terms; the other two are carried out in a similar manner. Considering the terms multiplying F_1, a direct substitution of the derivatives of $\boldsymbol{e}_1$ yields

$$\begin{aligned}
&\frac{\partial \boldsymbol{e}_1}{\partial t} + \frac{q_1}{l_1}\frac{\partial \boldsymbol{e}_1}{\partial \xi_1} + \frac{q_2}{l_2}\frac{\partial \boldsymbol{e}_1}{\partial \xi_2} - V_f\frac{\partial \boldsymbol{e}_1}{\partial n} \\
&\quad = \frac{1}{a_1}\left\{\frac{q_1^o}{a_2}\frac{\partial a_1}{\partial \xi_2} - \frac{\partial q_2^o}{\partial \xi_1}\right\}\boldsymbol{e}_2 + \left\{\frac{1}{a_1}\frac{\partial V_f}{\partial \xi_1} - \kappa_1 q_1^o\right\}\boldsymbol{n} + \frac{q_1}{l_1}\left(-\frac{1}{a_2}\frac{\partial a_1}{\partial \xi_2}\boldsymbol{e}_2 + a_1\kappa_1\boldsymbol{n}\right) \\
&\qquad + \frac{q_2}{l_2}\left(\frac{1}{a_1}\frac{\partial a_2}{\partial \xi_1}\boldsymbol{e}_2\right) \\
&\quad = \left\{\left(\frac{a_1 q_1}{l_1} - q_1^o\right)\kappa_1 + \frac{1}{a_1}\frac{\partial V_f}{\partial \xi_1}\right\}\boldsymbol{n} + \left\{\frac{1}{a_2}\frac{\partial a_1}{\partial \xi_2}\left(\frac{q_1^o}{a_1} - \frac{q_1}{l_1}\right) + \frac{q_2}{l_2}\frac{1}{a_1}\frac{\partial a_2}{\partial \xi_1} - \frac{1}{a_1}\frac{\partial q_2^o}{\partial \xi_1}\right\}\boldsymbol{e}_2.
\end{aligned}$$

Although we have accomplished the required decomposition, each of the two components can be further simplified by the repetitive use of (B 14) for q_1 and q_2, Lamé's relations (B 4) and the definition $l_1 = a_1(1 - n\kappa_1)$. We find that

$$\frac{\partial \boldsymbol{e}_1}{\partial t} + \frac{q_1}{l_1}\frac{\partial \boldsymbol{e}_1}{\partial \xi_1} + \frac{q_2}{l_2}\frac{\partial \boldsymbol{e}_1}{\partial \xi_2} - V_f\frac{\partial \boldsymbol{e}_1}{\partial n} = \frac{1}{l_1}\frac{\partial V_f}{\partial \xi_1}\boldsymbol{n} - \frac{l_2}{l_1}\frac{\partial}{\partial \xi_1}\left(\frac{q_2}{l_2}\right)\boldsymbol{e}_2,$$

$$\frac{\partial \boldsymbol{e}_2}{\partial t} + \frac{q_1}{l_1}\frac{\partial \boldsymbol{e}_2}{\partial \xi_1} + \frac{q_2}{l_2}\frac{\partial \boldsymbol{e}_2}{\partial \xi_2} - V_f\frac{\partial \boldsymbol{e}_2}{\partial n} = \frac{1}{l_2}\frac{\partial V_f}{\partial \xi_2}\boldsymbol{n} - \frac{l_1}{l_2}\frac{\partial}{\partial \xi_1}\left(\frac{q_1}{l_1}\right)\boldsymbol{e}_1,$$

$$\frac{\partial \boldsymbol{n}}{\partial t} + \frac{q_1}{l_1}\frac{\partial \boldsymbol{n}}{\partial \xi_1} + \frac{q_2}{l_2}\frac{\partial \boldsymbol{n}}{\partial \xi_2} = -\left\{\frac{1}{l_1}\frac{\partial V_f}{\partial \xi_1} + \frac{1}{l_2}\frac{\partial V_f}{\partial \xi_2}\right\}.$$

Therefore,

$$\begin{aligned}\frac{\partial \boldsymbol{F}}{\partial t} \mapsto & \frac{\partial \boldsymbol{F}}{\partial t} + (\boldsymbol{q}\cdot\nabla_s)\boldsymbol{F} - V_f\frac{\partial \boldsymbol{F}}{\partial n} \\ = & \left\{\frac{\partial F_1}{\partial t} + \boldsymbol{q}\cdot\nabla_s F_1 - V_f\frac{\partial F_1}{\partial n} - F_2\frac{l_1}{l_2}\frac{\partial}{\partial \xi_2}\left(\frac{q_1}{l_1}\right) - \frac{F_3}{l_1}\frac{\partial V_f}{\partial \xi_1}\right\}\boldsymbol{e}_1 \\ & + \left\{\frac{\partial F_2}{\partial t} + \boldsymbol{q}\cdot\nabla_s F_2 - V_f\frac{\partial F_2}{\partial n} - F_1\frac{l_2}{l_1}\frac{\partial}{\partial \xi_1}\left(\frac{q_2}{l_2}\right) - \frac{F_3}{l_2}\frac{\partial V_f}{\partial \xi_2}\right\}\boldsymbol{e}_2 \\ & + \left\{\frac{\partial F_3}{\partial t} + \boldsymbol{q}\cdot\nabla_s F_3 - V_f\frac{\partial F_3}{\partial n} + \frac{F_1}{l_1}\frac{\partial V_f}{\partial \xi_1} + \frac{F_2}{l_2}\frac{\partial V_f}{\partial \xi_2}\right\}\boldsymbol{n}.\end{aligned}$$

In the moving frame, the convective derivative of the velocity field

$$\frac{\mathrm{D}\boldsymbol{v}}{\mathrm{D}t} \equiv \frac{\partial \boldsymbol{v}}{\partial t} + \tfrac{1}{2}\nabla(\boldsymbol{v}\cdot\boldsymbol{v}) - \boldsymbol{v}\times(\nabla\times\boldsymbol{v}),$$

is obtained from

$$\begin{aligned}\frac{\mathrm{D}\boldsymbol{v}}{\mathrm{D}t} \mapsto & \left\{\frac{\partial v_1}{\partial t} + (\boldsymbol{v}_\perp + \boldsymbol{q})\cdot\nabla_s v_1 + (u - V_f)\frac{\partial v_1}{\partial n}\right. \\ & \left. + \frac{u v_1}{l_1}\frac{\partial l_1}{\partial n} - \frac{v_2}{l_1 l_2}\left(v_2\frac{\partial l_2}{\partial \xi_1} - v_1\frac{\partial l_1}{\partial \xi_2}\right) - v_2\frac{l_1}{l_2}\frac{\partial}{\partial \xi_2}\left(\frac{q_1}{l_1}\right) - \frac{u}{l_1}\frac{\partial V_f}{\partial \xi_1}\right\}\boldsymbol{e}_1 \\ & + \left\{\frac{\partial v_2}{\partial t} + (\boldsymbol{v}_\perp + \boldsymbol{q})\cdot\nabla_s v_2 + (u - V_f)\frac{\partial v_2}{\partial n} + \frac{u v_2}{l_2}\frac{\partial l_2}{\partial n}\right. \\ & \left. - \frac{v_1}{l_1 l_2}\left(v_1\frac{\partial l_1}{\partial \xi_2} - v_2\frac{\partial l_2}{\partial \xi_1}\right) - v_1\frac{l_2}{l_1}\frac{\partial}{\partial \xi_1}\left(\frac{q_2}{l_2}\right) - \frac{u}{l_2}\frac{\partial V_f}{\partial \xi_2}\right\}\boldsymbol{e}_2 \\ & + \left\{\frac{\partial u}{\partial t} + (\boldsymbol{v}_\perp + \boldsymbol{q})\cdot\nabla_s u + (u - V_f)\frac{\partial u}{\partial n} - \frac{v_1^2}{l_1}\frac{\partial l_1}{\partial n} - \frac{v_2^2}{l_2}\frac{\partial l_2}{\partial n} + \boldsymbol{v}_\perp\cdot\nabla_s V_f\right\}\boldsymbol{n}.\end{aligned} \tag{B 16}$$

REFERENCES

Addabbo, R., Bechtold, J. K. & Matalon, M. 2002 Wrinkling of spherically expanding flames. *Proc. Combust. Inst.* **29** (in press).

Batchelor, G. K. 1967 *An Introduction to Fluid Dynamics*. Cambridge University Press.

Bechtold, J. K. & Matalon, M. 1987 Hydrodynamics and diffusion effects on the stability of spherically expanding flames. *Combust. Flame* **67**, 77–90.

Bechtold, J. K. & Matalon, M. 1999 Effects of stoichiometry on stretched premixed flames. *Combust. Flame* **119**, 217–232.

Bechtold, J. K. & Matalon, M. 2001 The dependence of the Markstein length on stochiometry. *Combust. Flame* **127**, 1906–1913.

Bradley, D. 1999 Instabilities and flame speed in large-scale premixed gaseous explosions. *Phil. Trans. R. Soc. Lond.* A **357**, 3567–3581.

Bradley, D. & Harper, C. M. 1994 The development of instabilities in laminar explosion flames. *Combust. Flame* **99**, 562–573.

Buckmaster, J. & Crowley A. B. 1983 The fluid mechanics of flame tips. *J. Fluid Mech.* **131**, 341–361.

Buckmaster, J. D. & Ludford, G. S. S. 1982 *Theory of Laminar Flames*. Cambridge University Press.

Cheatham, S. & Matalon, M. 2000 A general asymptotic theory of diffusion flames with the application to cellular instability. *J. Fluid Mech.* **414**, 105–144.

Clavin, P. & Garcia, P. J. 1983 The influence of the temperature-dependence on the dynamics of flame fronts. *J. Méc. Theor. Appl.* **2**, 245–263.

Clavin, P. & Joulin, G. 1997 High-frequency response of premixed flames in weak stretch and curvature: a variable-density analysis. *Combust. Theory Modell.* **1**, 429–446.

Daou, J. & Matalon, M. 2001 Flame propagation in Poiseuille flow under adiabatic conditions. *Combust. Flame* **124**, 337–349.

Echekki, T. & Mungal, M. G. 1990 Flame speed measurements at the tip of a slot burner: effects of flame curvature and hydrodynamic stretch. *Twenty-Third Sympo. (Intl) on Combustion*, pp. 455–461. The Combustion Institute.

Eteng, E., Ludford, G. S. S. & Matalon, M. 1986 Displacement effect of a flame in a stagnation-point flow. *Phys. Fluids* **29**, 2172–2180.

Goldstein, S. 1938 *Modern Developments in Fluid Dynamics* Clarendon.

Ida, M. P. & Miksis, M. J. 1998 The dynamics of thin films I: General theory. *SIAM J. Appl. Maths* **58**, 456–473.

Jackson, T. L. 1987 Effects of thermal expansion on the stability of two-reactant flames. *Combust. Sci. Techol.* **53**, 51–54.

Joulin, G. 1994 On the response of premixed flames to time-dependent stretch and curvature. *Combust. Sci. Technol.* **97**, 219–229.

Joulin, G. & Mitani, T. 1981 Linear stability analysis of two-reactant flames. *Combust. Flame* **40**, 235–246.

Keller, D. & Peters, N. 1994 Transient pressure effects in the evolution equation for premixed flame fronts. *Theor. Comput. Fluid Dyn.* **6**, 141–159.

Kim, Y. & Matalon, M. 1990 On the stability of near-equidiffusional strained premixed flames. *Combust. Sci. Techol.* **69**, 85–97.

Kwon, S., Tseng, L. K. & Faeth G. M. 1992 Laminar burning velocities and transition to unstable flames in $H_2/O_2/N_2$ and $C_3H_8/O_2/N_2$ mixtures. *Combust. Flame* **90**, 230–246.

Lamé, G. 1859 *Leçons sur les Coordonnées Curvilignes et leurs Diverses Applications.* Mallet-bachelier Imprimeur-Libraire, Paris.

Lewis, B. & von Elbe, G. 1987 *Combustion, Flames and Explosions of Gases*, 3rd Edn. Academic.

Matalon, M. 1983 On flame stretch. *Combust. Sci. Technol.* **31**, 169–182.

Matalon, M. & Matkowsky, B. J. 1982 Flames as gasdynamic discontinuities. *J. Fluid Mech.* **124**, 239–259.

Matalon, M. & Matkowsky, B. J. 1983 Flames in fluids: their interactions and stability. *Combust. Sci. Techol.* **34**, 295–316.

Matalon, M. & Matkowsky, B. J. 1984 On the stability of plane and curved flames. *SIAM J. Appl. Maths* **44**, 327–343.

Mitani, T. 1980 Propagation velocities of two-reactant flames. *Combust. Sci. Techol.* **21**, 175–177.

Pelce, P. & Clavin, P. 1982 Influence of hydrodynamics and diffusion upon the stability limits of laminar premixed flames. *J. Fluid Mech.* **124**, 219–237.

Peters, N. 2000 *Turbulent Combustion*, Cambridge University Press.

Quinard, J., Searby, G. & Boyer, L. 1984 Cellular structures on premixed flames in a uniform laminar flow. In *Cellular Structures in Instabilities.* Lecture Notes in Physics, vol. 210, pp. 331–341. Springer.

Rosenhead, L. 1963 *Laminar Boundary Layers.* Oxford University Press.

Searby, G. & Quinard, J. 1990 Direct and indirect measurements of Markstein numbers of premixed flames. *Combust. Flame* **82**, 298–311.

Sen, A. K. & Ludford, G. S. S. 1979 The near-stoichiometric behaviour of combustible mixtures part 1: diffusion of the reactants. *Combust. Sci. Technol.* **21**, 15–23.

Strehlow, R. A. 1984 *Fundamentals of Combustion* 2nd Edn. McGraw-Hill.

Struik, D. J. 1961 *Lectures on Classical Differential Geometry.* Dover.

Tien, J. H. & Matalon, M. 1991 On the burning velocity of stretched flames. *Combust. Flame* **84**, 238–248.

Uberoi, M. S., Kuethe, A. M. & Menkes. H. R. 1958 Flow field of a Bunsen flame. *Phys. Fluids* **1**, 150–158.

Weatherburn, C. E. 1961 *Differential Geometry of Three Dimensions.* Cambridge University Press. vol. 1: 207–215.

Westbrook, C. K. & Dryer, F. T. 1981 Simplified reaction mechanisms for the oxidation of hydrocarbon fuels in flames. *Combust. Sci. Technol.* **27**, 31–43.

Williams, F. A. 1985 *Combustion Theory* 2nd Edn. Benjamin Cummings.

Wu, C. K. & Law, C. K. 1984 On the determination of laminar flame speeds from stretched flames. *Twentieth Sympo. (Intl) on Combustion*, pp. 1941–1949. The Combustion Institute.

Yao, J. & Stewart, S. 1996 On the dynamics of multi-dimensional detonation. *J. Fluid Mech.* **309**, 225–275.